Electronic Supplementary Material (ESI) for Journal of Materials Chemistry C.

Table of contents:

1. General experimental procedures

If not stated otherwise, all reactions and manipulations were carried out under an atmosphere of dry nitrogen using Schlenk techniques or in an inert-atmosphere glovebox. *n*-Hexane, toluene, and THF were distilled from Na/benzophenone prior to use. BBr_3 was stored over Hg to remove contaminations with Br_2. Organic compounds for OLED-device fabrication were purchased from *Jilin OLED Material Tech Co., Ltd* and used without further purification. 4,5-Difluoro-1,2-bis(trimethylsilyl)benzene,[S1] and the reported B-PAHs $\mathbf{3^H}$[S2] and $\mathbf{3^{Cl}}$[S2] were prepared according to literature procedures.

NMR spectra were recorded at 298 K using the following spectrometers: *Bruker* Avance-300 or Avance-500 spectrometer. Chemical shift values are referenced to (residual) solvent signals ($^1H/^{13}C\{^1H\}$; $CDCl_3$: δ = 7.26/77.16 ppm) or external $BF_3{\cdot}Et_2O$ ($^{11}B\{^1H\}$: 0.00 ppm) and external $CFCl_3$ ($^{19}F\{^1H\}/^{19}F$: 0.00 ppm). Abbreviations: s = singlet, d = doublet, dd = doublet of doublets, m = multiplet, br. = broad. Resonances of carbon atoms attached to boron atoms were typically broadened and sometimes not observed due to the quadrupolar relaxation of boron. Boron resonances of triarylborane compounds are typically very broad ($h_{1/2}$ > 1100 Hz) and were observed only in highly concentrated samples. Resonance assignments were aided by ^{H,H}COSY, ^{H,C}HSQC, and, if necessary, also ^{H,C}HMBC spectra.

UV/Vis absorption spectra were recorded at room temperature using a *Varian* Cary 60 Scan UV/Vis spectrophotometer. Photoluminescence (PL) spectra in solution were recorded at room temperature using a *Jasco* FP-8300 spectrofluorometer equipped with a calibrated *Jasco* ILF-835 100 mm diameter integrating sphere and analyzed using the *Jasco* FWQE-880 software. For PL quantum yield (Φ_{PL}) measurements in solution, each sample was carefully degassed with argon using an injection needle and a septum-capped cuvette. Under these conditions, the Φ_{PL} of the fluorescence standard 9,10-diphenylanthracene was determined as 97% (lit.: 97%).[S3,S4] For all Φ_{PL} measurements in solution, at least three samples of different concentrations were used (range between 10^{-5} and 10^{-7} mol L^{-1}). Due to self-absorption, slightly lower Φ_{PL} values were observed at higher concentrations. This effect was corrected by applying a method reported by *Bardeen et al.*, which slightly improved the Φ_{PL} values (4% at most).[S5] PL spectra and PL decay lifetimes of neat, solid B-PAHs were recorded at room temperature using an *Edinburgh Instruments* FLS980 spectrophotometer equipped with 365 nm picosecond pulsed LEDs and analyzed using the *Edinburgh Instruments* F980 software. Φ_{PL} of neat, solid B-PAHs were recorded using a *Hamamatsu Photonics K.K.* absolute PL quantum yield spectrometer C11347-11 and analyzed using the *Hamamatsu Photonics K.K.* U6039-05 software. Cyclic voltammetry (CV) measurements were performed in a glovebox at room temperature in a one-chamber, three-electrode cell using an *EG&G* Princeton Applied Research 263A potentiostat. A platinum disk electrode (2.00 mm diameter) was used as the working electrode with a platinum wire counter electrode and a silver wire reference electrode, which was coated with AgCl by immersion into HCl/HNO_3 (3:1). Prior to measurements, the solvent THF was dried with NaK. [nBu$_4$N][PF_6] (*Sigma Aldrich*; used as received) was employed as the supporting electrolyte (0.1 mol L^{-1}). All potential values were referenced against the FcH/FcH^+ redox couple (FcH = ferrocene; $E_{1/2}$ = 0 V). Scan rates were varied between 100 and 400 mV s^{-1}. High-resolution mass spectra were measured in positive mode using a *Thermo Fisher Scientific* MALDI LTQ Orbitrap XL spectrometer and α-cyano-4-hydroxycinnamic acid as the matrix.

2. Nomenclature

To maintain consistency with previous publications, the NMR signals were assigned according to the numbering scheme below, which differs from the IUPAC numbering scheme underlying the systematic names.

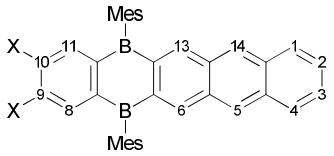

3. Synthesis, purification methods, and analytical data

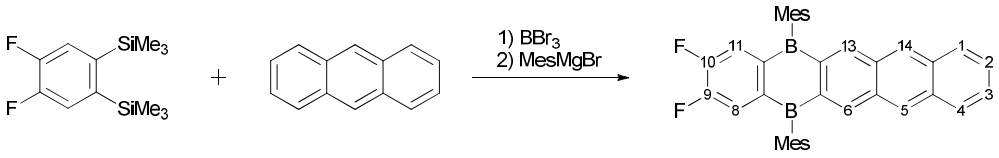

Synthesis of the fluorinated anthracene derivative 3^F: A thick-walled glass ampoule was charged with 4,5-difluoro-1,2-bis(trimethylsilyl)benzene (0.500 g, 1.93 mmol), anthracene (0.690 g, 3.87 mmol), BBr_3 (0.57 mL, 1.5 g, 6.0 mmol), and *n*-hexane (5 mL) as the solvent. The ampoule was flame-sealed under vacuum and subsequently heated to 120 °C for 2.5 d. The BBr precursor of $\mathbf{3^F}$ crystallized already in the reaction ampoule in the form of small red plates that were suitable for an X-ray crystal structure analysis. The obtained dark red solution including the crystals, was cooled to room temperature, transferred to a Schlenk tube and evaporated to dryness under a dynamic vacuum. The solid residue was dissolved in toluene (20 mL) and stirred at a reduced pressure of 25 torr for 1 h to remove residual BBr_3 (the volume of the solution decreases only slightly). A solution of MesMgBr in THF (0.80 M, 4.9 mL, 3.9 mmol) was added dropwise with stirring over 2 min at 0 °C. The reaction mixture was allowed to warm to room temperature overnight, quenched with aqueous saturated $NaHCO_3$ (100 mL), and the organic phase was separated with a separation funnel. The aqueous phase was extracted with $CHCl_3$ (3 × 25 mL). The organic phases were combined, washed with H_2O (20 mL), dried over anhydrous $MgSO_4$, and filtered. All volatiles were removed from the filtrate under reduced pressure. The purification of the crude product by column chromatography (14 cm silica gel, d = 5 cm, eluent: cyclohexane, R_f = 0.25) afforded $\mathbf{3^F}$ as a yellow solid. Yield: 0.279 g (0.509 mmol, 26%). Single crystals of $\mathbf{3^F}$ were grown from hot toluene.

^{1}H NMR (500.2 MHz, $CDCl_3$): δ = 8.42 (s, 2H; H-5,14), 8.41 (s, 2H; H-6,13), 7.97-7.95 (m, 2H; H-1,4), 7.54-7.52 (m, 2H; H-8,11), 7.52-7.50 (m, 2H; H-2,3), 7.03 (s, 4H; Mes-CH-*m*), 2.49 (s, 6H; Mes-CH_3-*p*), 2.15 ppm (s, 12H; Mes-CH_3-*o*)
^{13}C{^{1}H} NMR (125.8 MHz, $CDCl_3$): δ = 153.9 (dd, ^1J(C,F) = 260.3 Hz, ^2J(C,F) = 13.8 Hz; C-9,10), 145.4 (br.; C-7a,11a), 144.1 (C-6,13), 140.4 (br.; Mes-C-*i*), 139.3 (br.; C-6a,12a), 138.5 (Mes-C-*o*), 137.3 (Mes-C-*p*), 133.5 (C-4a,14a), 133.1 (C-5a,13a), 129.6 (C-5,14), 128.8 (C-1,4), 127.4-127.3 (m; C-8,11), 127.3 (Mes-CH-*m*), 127.0 (C-2,3), 23.0 (Mes-CH_3-*o*), 21.5 ppm (Mes-CH_3-*p*)
^{11}B{^{1}H} NMR (160.5 MHz, $CDCl_3$): δ = 78 ppm ($h_{1/2} \approx$ 1500 Hz)
^{19}F{^{1}H} NMR (282.3 MHz, $CDCl_3$): δ = −131.5 ppm
^{19}F NMR (282.3 MHz, $CDCl_3$): δ = −(131.47-131.54) ppm (m, 2F; F-9,10)
HRMS: Calculated m/z for $[C_{38}H_{32}B_2F_2]^+$: 548.26527, found: 548.26522
UV-vis (C_6H_{12}): λ_{max} (ε) = 380 (4800), 407 (5900), 431 (13600), 458 nm (22400 $mol^{-1}dm^3cm^{-1}$)
Fluorescence (C_6H_{12}, λ_{Ex} = 407 nm): λ_{max} = 465, 494, 529, 568 nm; Φ_{PL} = 86%
Fluorescence (neat, λ_{Ex} = 396 nm): λ_{max} = 539 nm; Φ_{PL} = 5%
Photoluminescence decay (neat, λ_{Ex} = 365 nm): τ_i (A_i) = 1.52 (69.62), 6.39 ns (30.38%)
Cyclic voltammetry (THF, [nBu$_4$N][PF$_6$] 0.1 M, 200 mV s^{-1}, vs. FcH/FcH$^+$): $E_{1/2}$ = −1.84 V

4. Plots of ^{1}H, $^{11}B\{^{1}H\}$, $^{13}C\{^{1}H\}$, $^{19}F\{^{1}H\}$, and ^{19}F NMR spectra

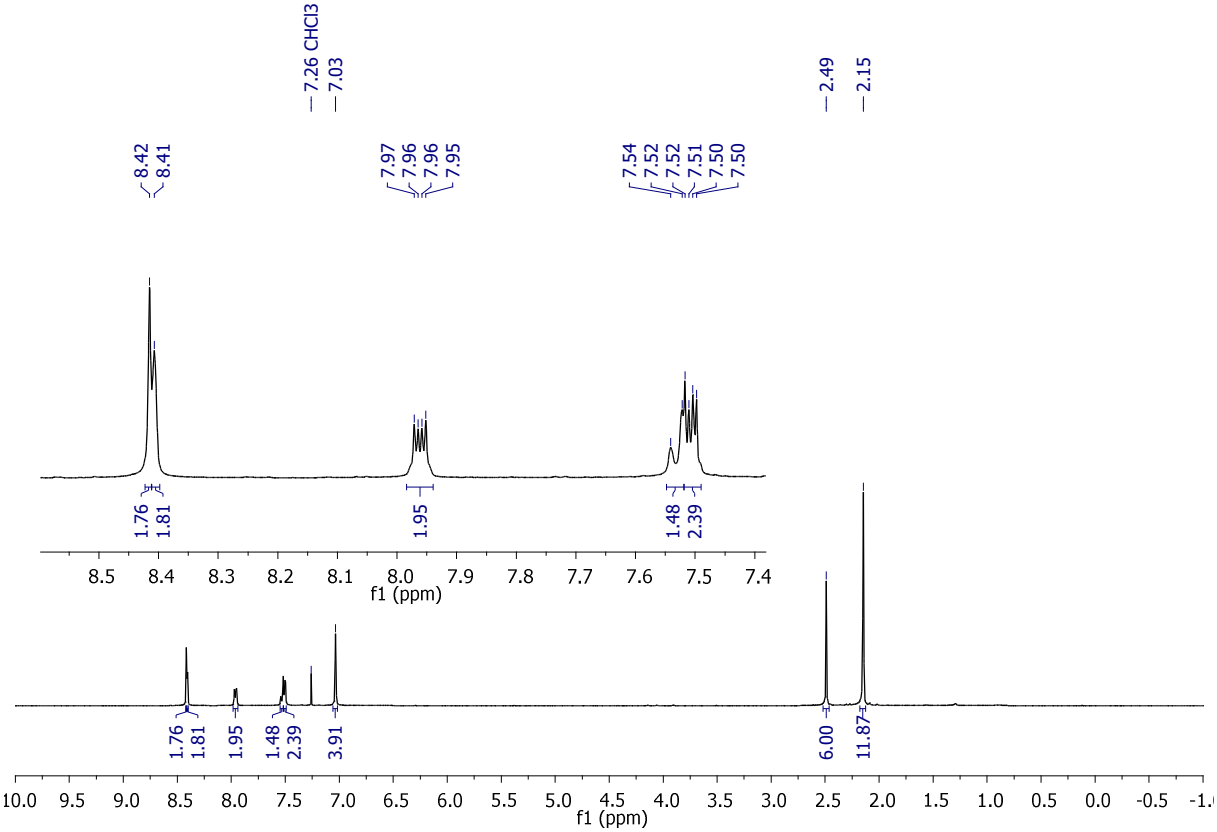

Figure S1: ^{1}H NMR spectrum of **3^{F}** ($CDCl_3$, 500.2 MHz).

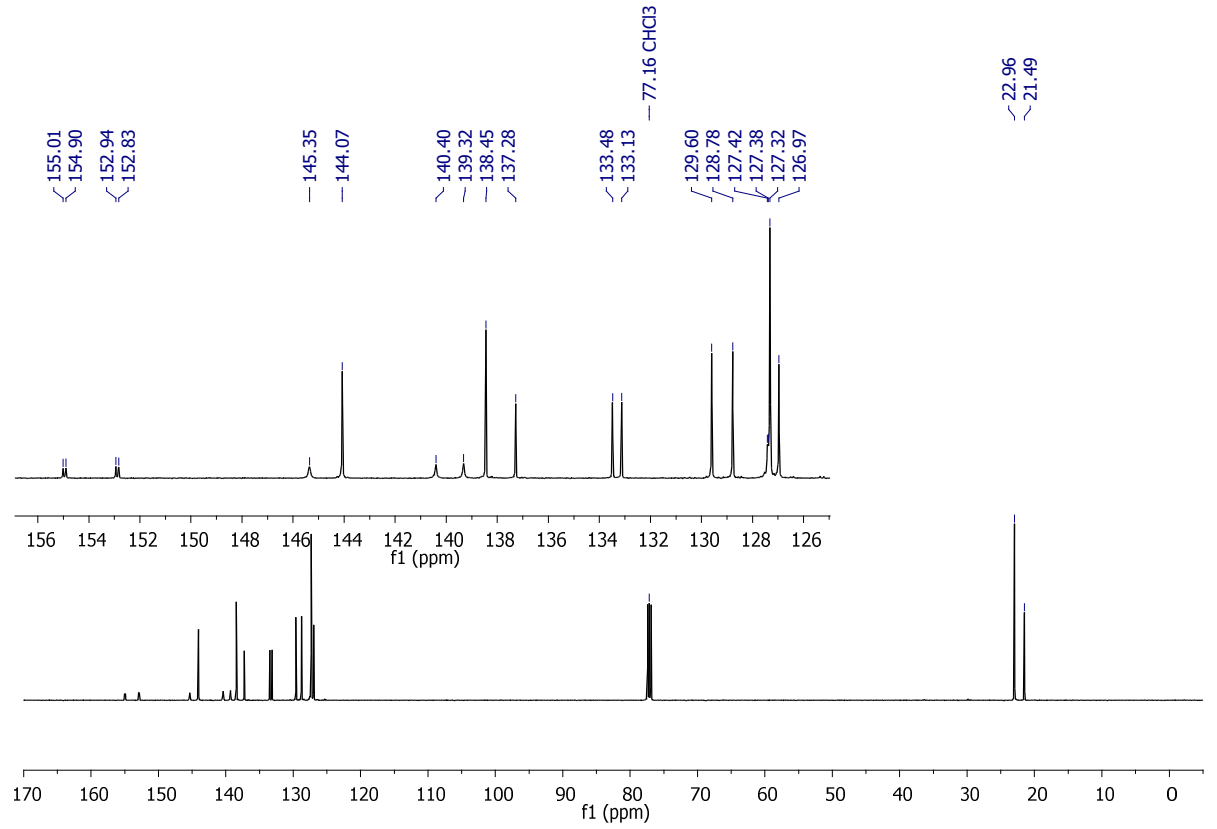

Figure S2: $^{13}C\{^{1}H\}$ NMR spectrum of **3^{F}** ($CDCl_3$, 125.8 MHz).

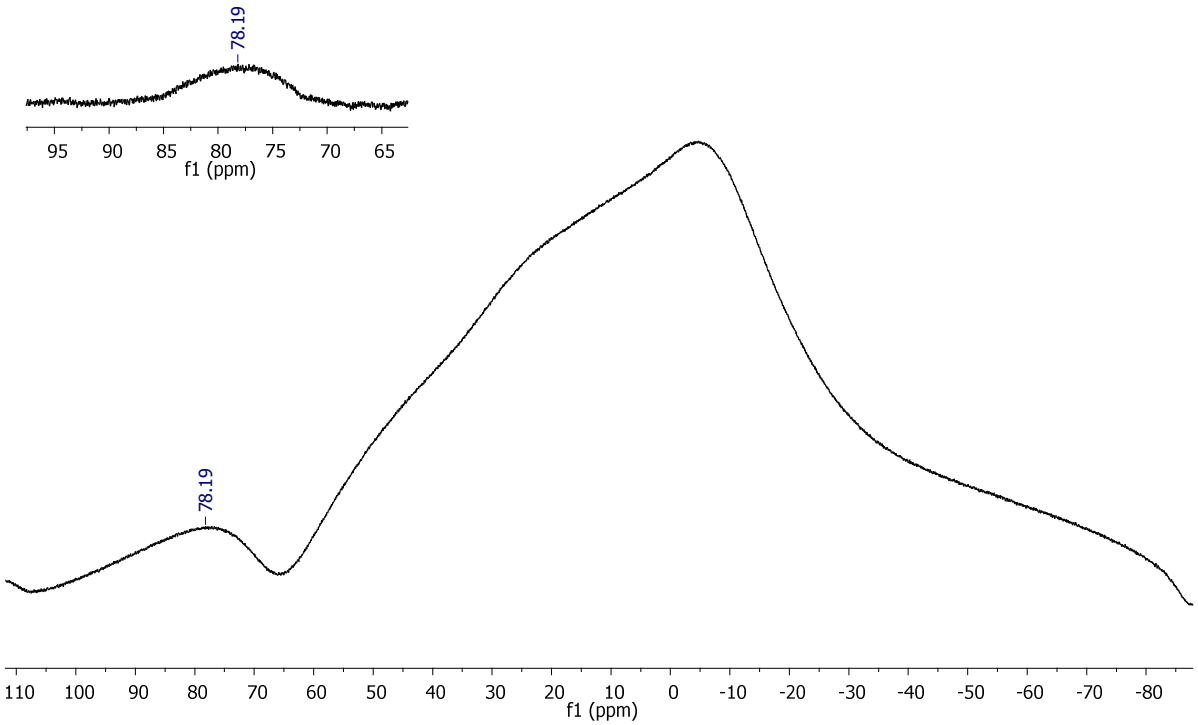

Figure S3: $^{11}B\{^{1}H\}$ NMR spectrum of **3^{F}** ($CDCl_3$, 160.5 MHz). *Note:* A baseline correction has only been performed for the inset.

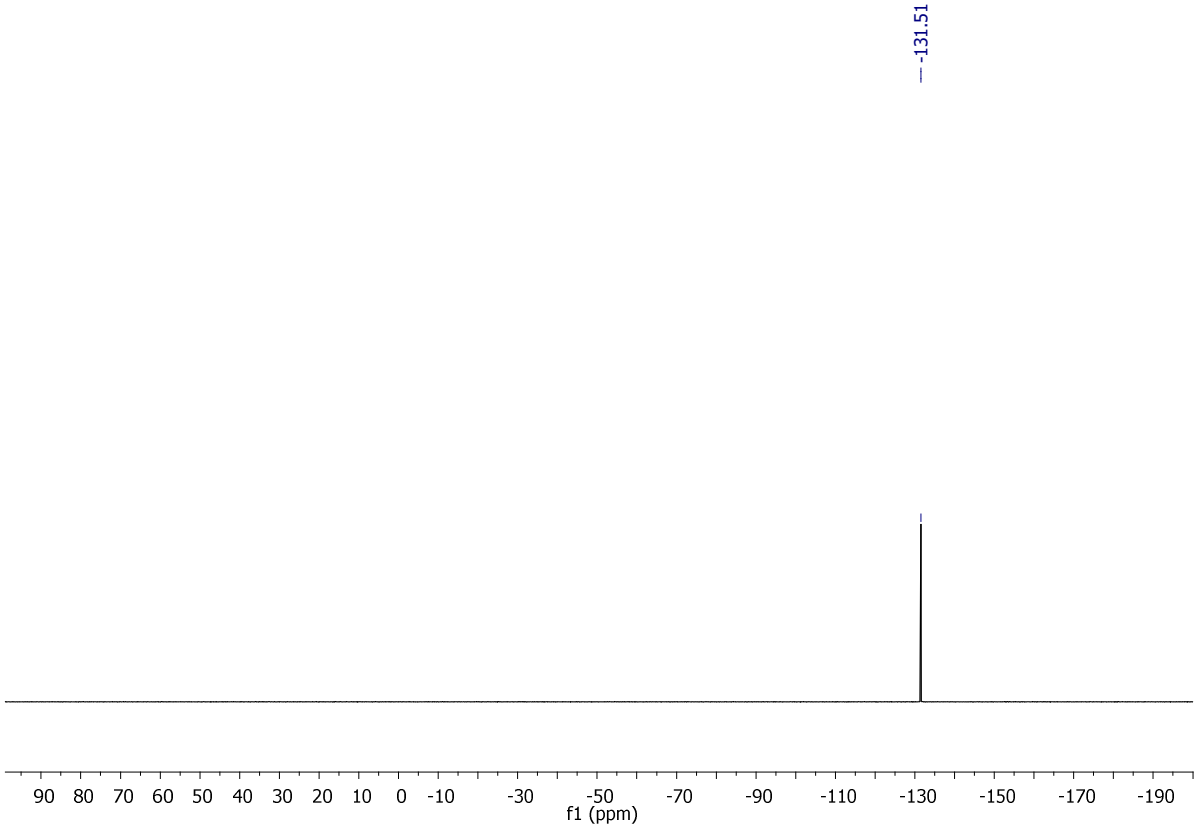

Figure S4: $^{19}F\{^{1}H\}$ NMR spectrum of **3^{F}** ($CDCl_3$, 282.3 MHz).

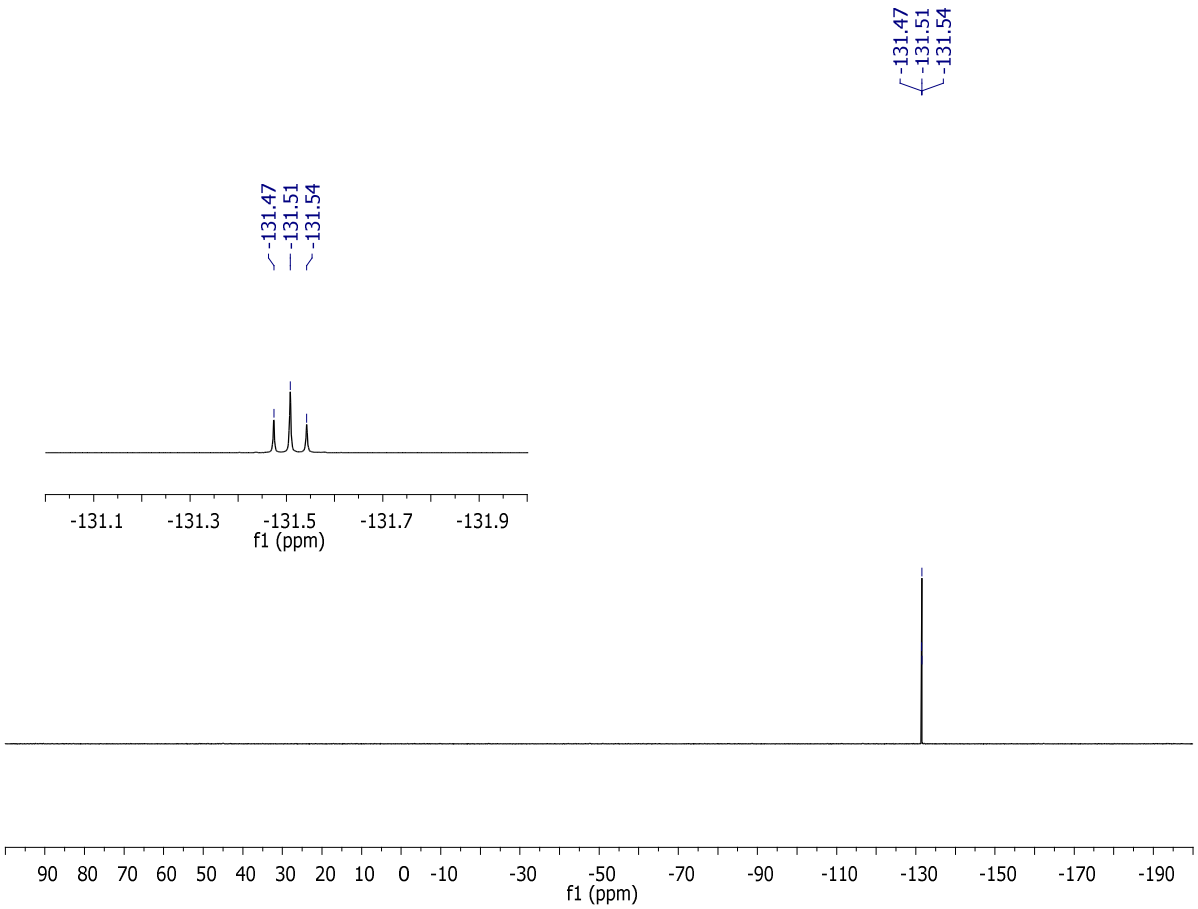

Figure S5: ^{19}F NMR spectrum of **3^{F}** ($CDCl_3$, 282.3 MHz).

5. Discussion of selected NMR spectra

In the ^{11}B{^{1}H}-NMR spectrum, the target product **3^{F}** gives rise to a broad resonance at δ = 78 ppm, which is in the range typically observed for triarylboranes.[S6] In contrast to the ^{1}H-NMR spectrum of **3^{Cl}**, the proton resonance of the halogenated *ortho*-phenylene ring in **3^{F}** appears as a multiplet due to coupling with the *ortho*-fluorine atoms. For **3^{H}**-**3^{Cl}**, the diborylated anthryl fragments invariably give rise to two singlets for the internal benzene rings and two multiplets for the peripheral benzene ring in the ^{1}H-NMR spectra. The ^{13}C{^{1}H}-NMR spectrum of **3^{F}** is as expected; the carbon atoms attached to boron are broadened. In the ^{19}F{^{1}H}-NMR spectrum, one signal at δ = –131.5 ppm is detected.

6. Photophysical and electrochemical data

Table S1. Photophysical and electrochemical data of the B-PAHs **3H**, **3F**, and **3Cl**.

Cmpd	λ_{abs}[a] (nm) (ε [M^{-1} cm^{-1}])	λ_{onset}[b] (nm)	λ_{ex} (nm)		λ_{em}[a] (nm)		Φ_{PL}[c] (%)		τ_{ave}[d] (ns)	Stokes shift[e] (cm^{-1})	E_{HOMO}/E_{LUMO}[f] (eV)	$E_{1/2}$ (V)	E_G^{opt}[g] (eV)
	C_6H_{12}	C_6H_{12}	C_6H_{12}	neat	C_6H_{12}	neat	C_6H_{12}	neat	neat	C_6H_{12}		THF	
3H	380 (4100) 402 (4800) 425 (9500) 452 (15400)	463	335	396	456 486 520	511 541	87	2	2.64	194	−5.49/−2.81	−1.99	2.68
3F	380 (4800) 407 (5900) 431 (13600) 458 (22400)	470	407	396	465 494 529 568	539	86	5	4.67	329	−5.60/−2.96	−1.84	2.64
3Cl	412 (2700) 437 (6900) 465 (11000)	475	339	396	470 501 537	529 564	90	26	5.45	229	−5.60/−2.99	−1.81	2.61

[a] Resolved vibrational fine structures. [b] Each onset wavelength (λ_{onset}) was determined by constructing a tangent on the point of inflection of the bathochromic slope of the most red-shifted absorption maximum. [c] Quantum yields were determined by using a calibrated integrating sphere. [d] Average lifetimes τ_{ave} are calculated according to the equation: $\Sigma A_i \tau_i^2 / \Sigma A_i \tau_i$, where A_i is the pre-exponential for the corresponding lifetime τ_i. [e] Stokes shifts represent the difference between each longest wavelength absorption maximum and the corresponding shortest wavelength emission maximum. [f] $E_{HOMO} = E_{LUMO} - E_G^{opt}$, $E_{LUMO} = -4.80$ eV$-E_{1/2}^{Red1}$ (FcH/FcH$^+$ = −4.80 eV vs. vacuum level). [g] Optical band gap $E_G^{opt} = 1240/\lambda_{onset}$.

6.1 UV-vis absorption and emission spectra

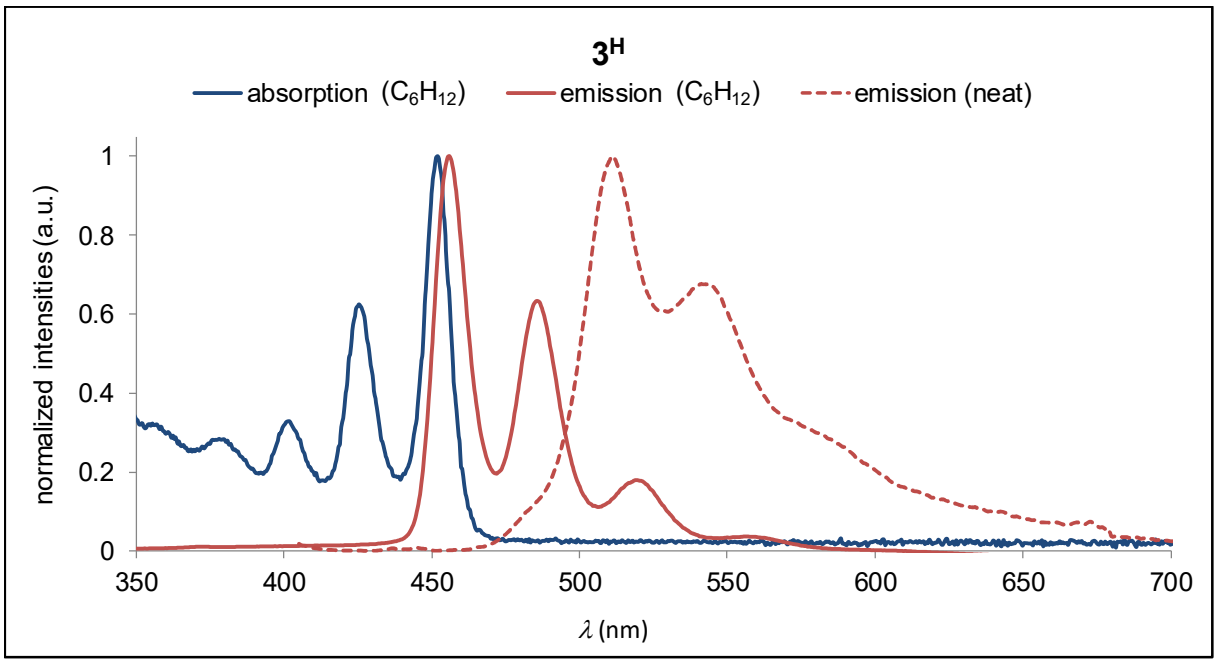

Figure S6: Normalized UV-vis absorption and emission spectra of **3H**.

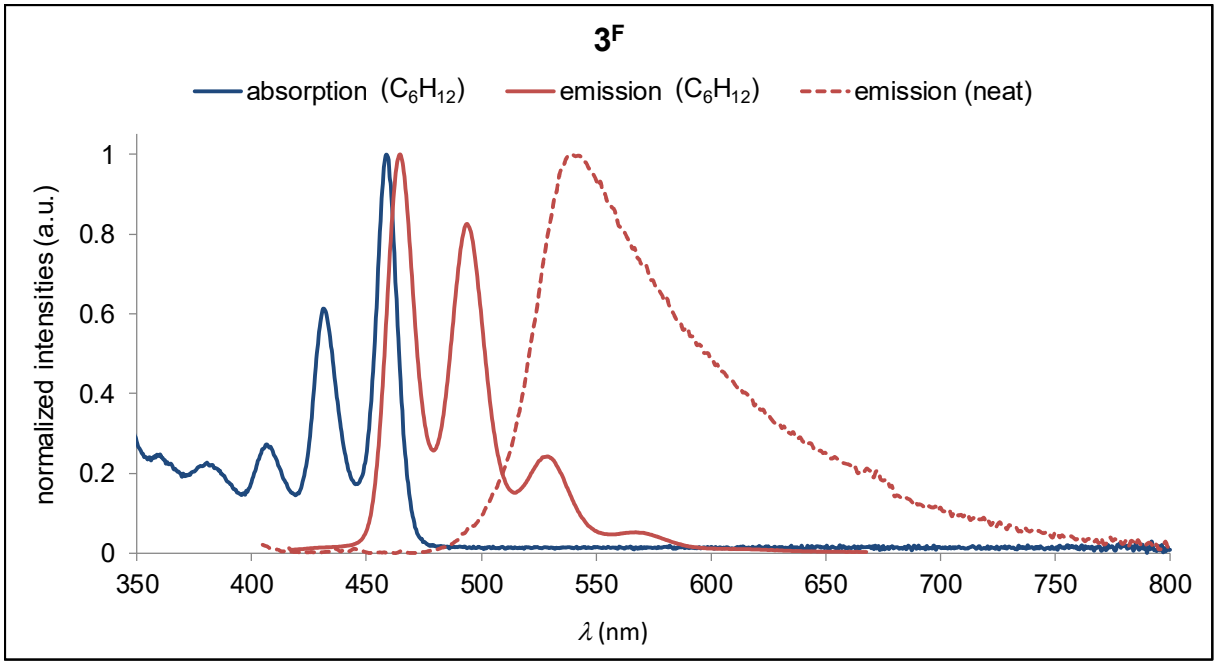

Figure S7: Normalized UV-vis absorption and emission spectra of $\mathbf{3^F}$.

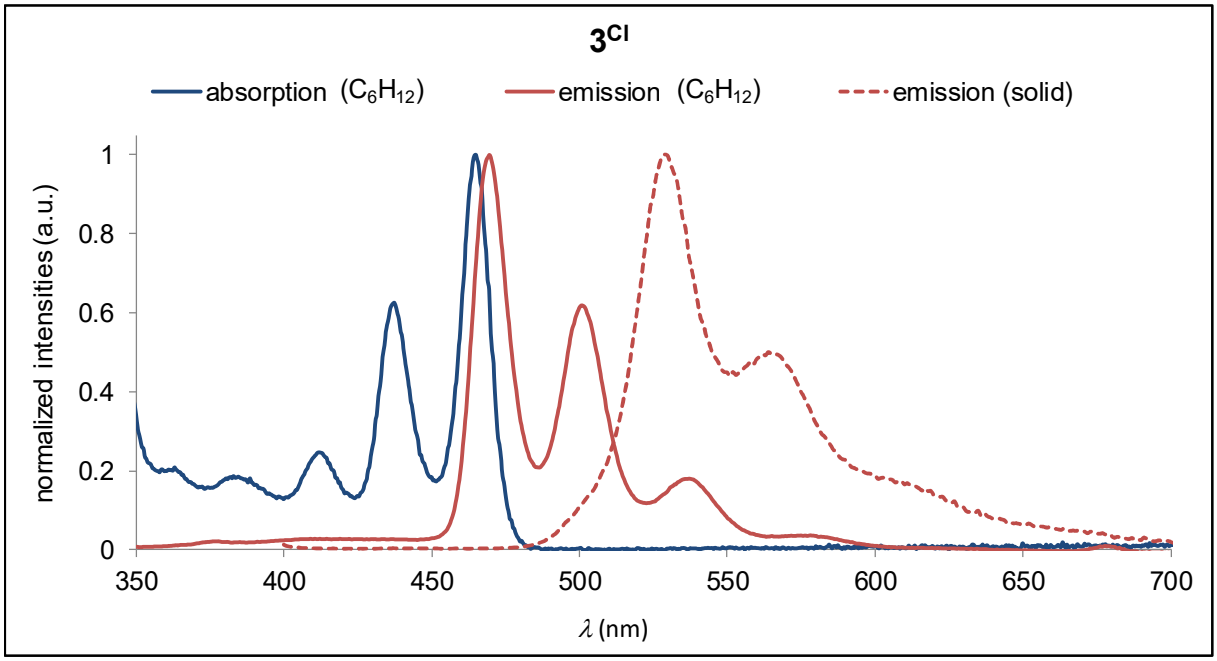

Figure S8: Normalized UV-vis absorption and emission spectra of $\mathbf{3^{Cl}}$.

6.2 Plot of the cyclic voltammogram

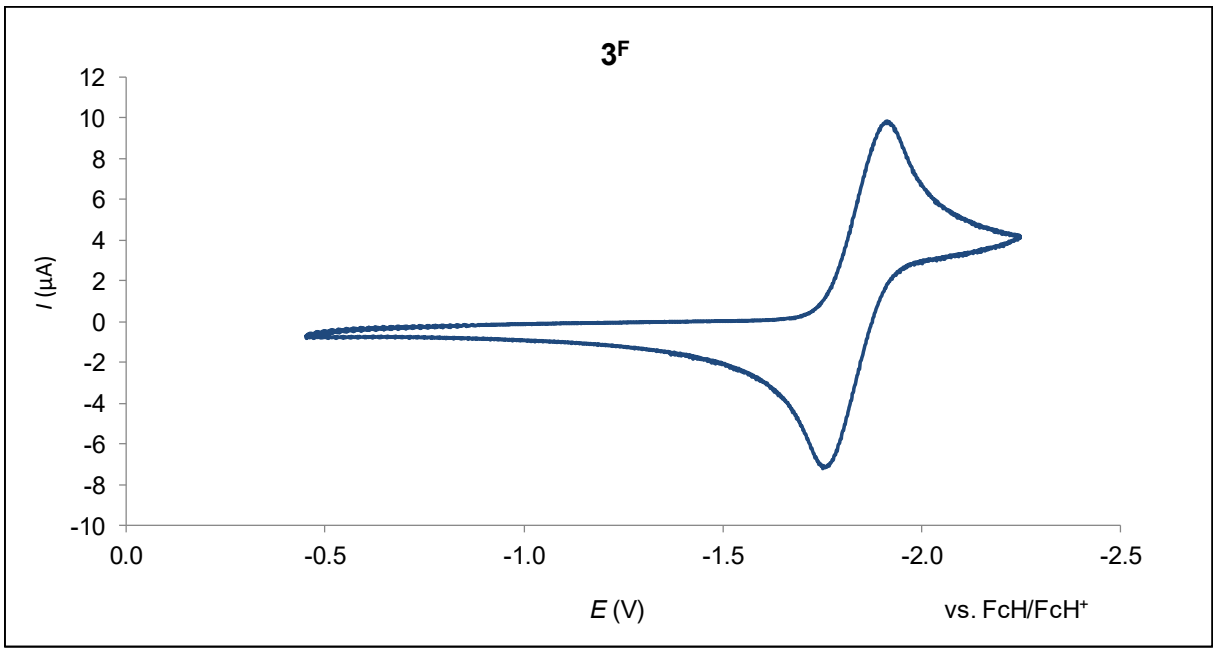

Figure S9: Cyclic voltammogram of **3F** in THF (room temperature, supporting electrolyte: [*n*Bu$_4$N][PF$_6$] (0.1 M), scan rate 200 mV s^{-1}).

6.3 Photoluminescent decay curves

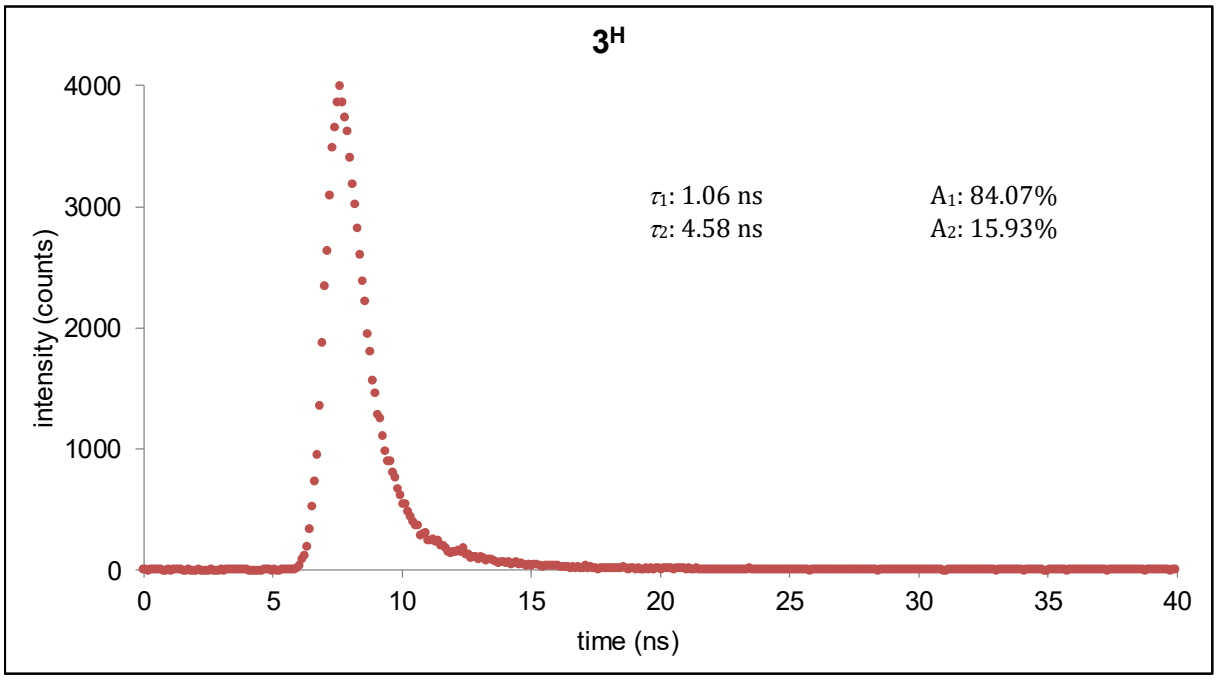

Figure S10: Photoluminescence decay lifetime of neat **3H** (room temperature).

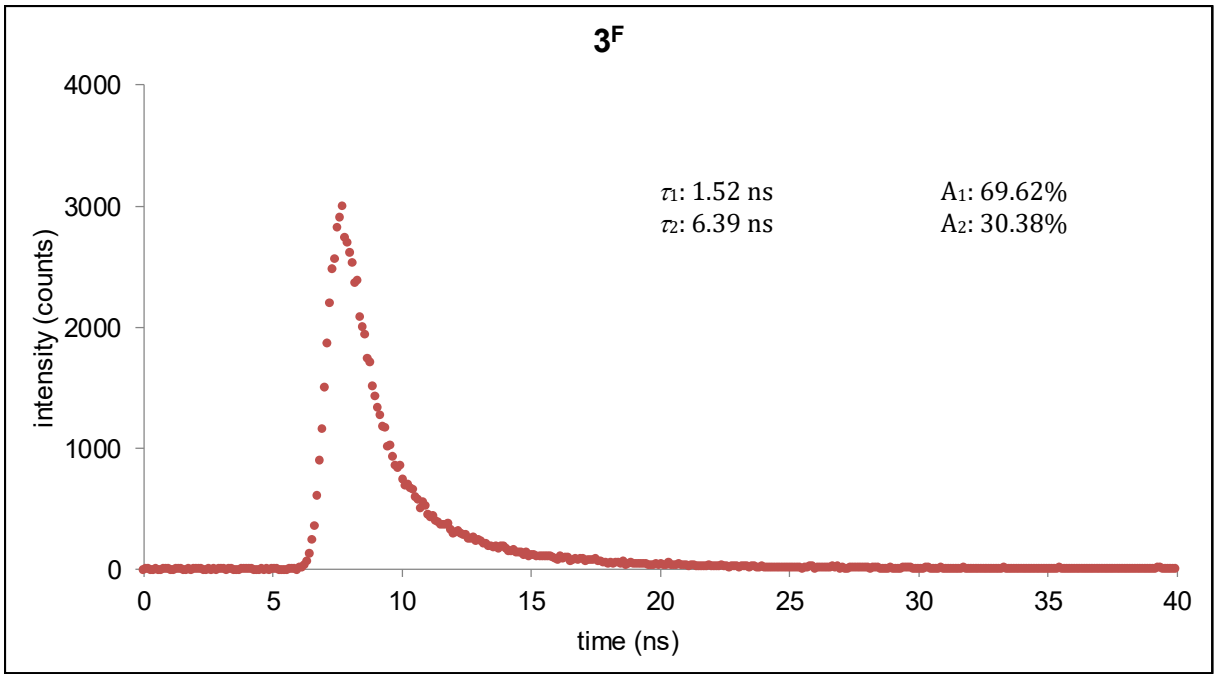

Figure S11: Photoluminescence decay lifetime of neat **3F** (room temperature).

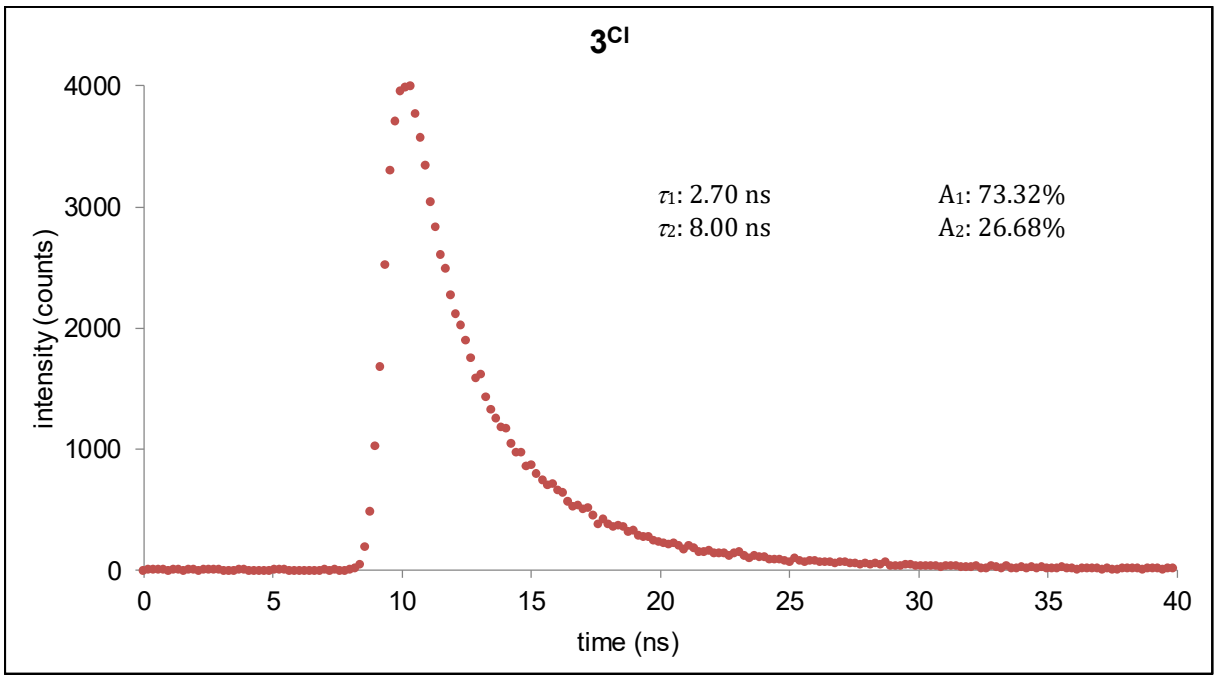

Figure S12: Photoluminescence decay lifetime of neat **3Cl** (room temperature).

7. X-ray crystal structure analyses

Data for all structures were collected on a STOE IPDS II two-circle diffractometer with a Genix Microfocus tube with mirror optics using MoK_α radiation (λ = 0.71073 Å) and were scaled using the frame scaling procedure in the *X-AREA*[S7] program system. The structures were solved by direct methods using the program *SHELXS*[S8] and refined against F^2 with full-matrix least-squares techniques using the program *SHELXL-97*.[S8]

CCDC files 1859549 (**3**$^{\mathbf{F*}}$) and 1859550 (**3**$^{\mathbf{F}}$(tol)) contain the supplementary crystallographic data for this paper and can be obtained free of charge from The Cambridge Crystallographic Data Centre via www.ccdc.cam.ac.uk/data_request/cif.

The crystal structures of **3**$^{\mathbf{H}}$(tol) (CCDC 1532059) and **3**$^{\mathbf{Cl}}$(tol)$_{1.5}$ (CCDC 1532050) have been reported in a previous publication.[S2]

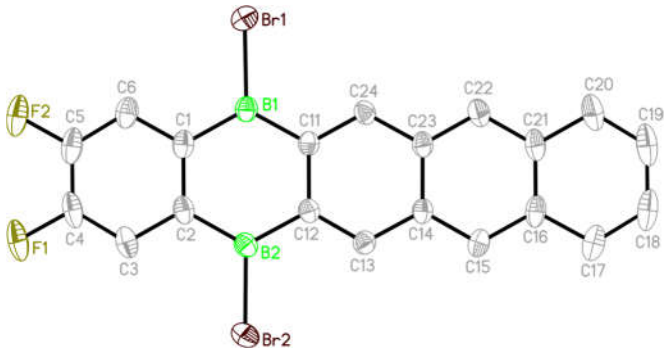

Figure S13 (CCDC 1859549): Molecular structure of **3^{F*}** in the solid state. Displacement ellipsoids are drawn at the 50% probability level; hydrogen atoms are omitted to clarity. Selected bond lengths [Å], bond angles [°], and torsion angles [°]: B1-C1 = 1.563(4), B1-C11 = 1.536(4), C1-C2 = 1.419(4), C4-F1 = 1.359(3); C1-B1-C11 = 122.4(2), C11-B1-Br1 = 119.45(18); B1-C11-C24-C23 = 177.7(2), C13-C14-C15-C16 = 178.3(2).

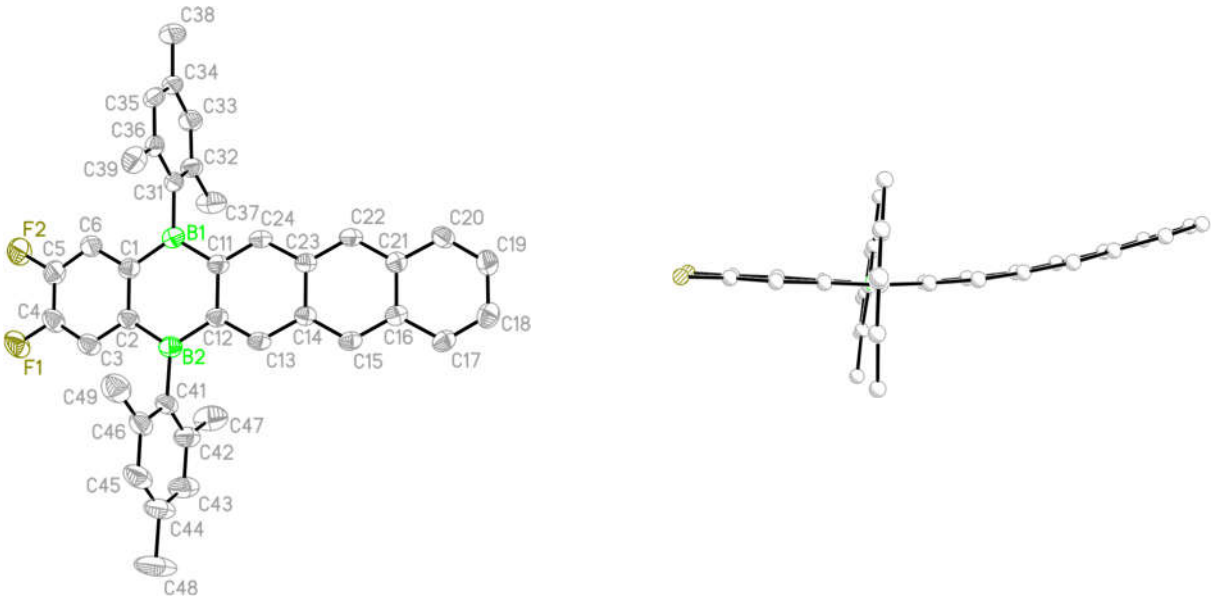

Figure S14 (CCDC 1859550): Molecular structure of **3^{F}**(tol) in the solid state. Displacement ellipsoids are drawn at the 50% probability level; hydrogen atoms are omitted to clarity. Selected bond lengths [Å], bond angles [°], and torsion angles [°]: B1-C1 = 1.565(3), B1-C11 = 1.556(3), C1-C2 = 1.420(3), C4-F1 = 1.359(3); C1-B1-C11 = 118.25(19), C11-B1-C31 = 121.99(19); C11-B1-C31-C32 = 87.0(3), C1-B1-C31-C36 = 89.1(3), B1-C11-C24-C23 = −173.1(2), C13-C14-C15-C16 = 172.55(19).

Table S2: Selected crystallographic data for **3^{F*}**, and **3^{F}**(tol).

compound	**3^{F*}**	**3^{F}**(tol)
CCDC	1859549	1859550
formula	$C_{20}H_{10}B_2Br_2F_2$	$C_{38}H_{32}B_2F_2$ x C_7H_8
M_r	469.72	640.39
T (K)	173(2)	173(2)
radiation, λ (Å)	Mo$K\alpha$, 0.71073	Mo$K\alpha$, 0.71073
crystal system	triclinic	monoclinic
space group	$P\,{-}1$	$P\,2_1/c$
a (Å)	7.2783(7)	20.3634(14)
b (Å)	9.6835(8)	7.6539(4)
c (Å)	12.2806(11)	24.5216(16)
α (°)	85.371(7)	90
β (°)	83.085(7)	108.846(5)
γ (°)	87.911(7)	90
V (Å^3)	856.12(13)	3617.0(4)
Z	2	4
D_{calcd} (g cm^{-3})	1.822	1.176
F(000)	456	1352
μ (mm^{-1})	4.755	0.073
crystal size (mm)	0.120 x 0.040 x 0.020	0.250 x 0.130 x 0.130
crystal color, form	red plate	yellow needle
reflections collected	10049	38952
independent reflections	4388	6376
R_{int}	0.0318	0.0744
data/restraints/parameters	4388/0/235	6376/0/449
R_1, wR_2 (I > 2σ(I))	0.0372, 0.0900	0.0505, 0.1032
R_1, wR_2 (all data)	0.0520, 0.0961	0.0997, 0.1184
Goodness-of-fit on F^2	1.008	0.920
largest diff peak and hole (e Å^{-3})	0.676, −0.649	0.149, −0.192

8. Computational details and HOMO/LUMO analyses

Geometry optimizations and frequency calculations were carried out with the Gaussian 09 software package[S9] using the B3LYP functional and the 6-31G* basis set. The stationary points were characterized as minima (no imaginary frequencies in the vibrational analysis). The graphics were produced with Avogadro 1.1.1 and POV-Ray 3.7.0.

8.1 Computational details and HOMO/LUMO analyses for the B-PAH 3^{F} calculated at the B3LYP/6-31G* level

3^{F} (ΔE = 3.16 eV)	
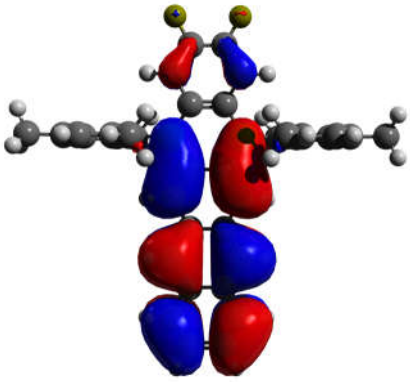	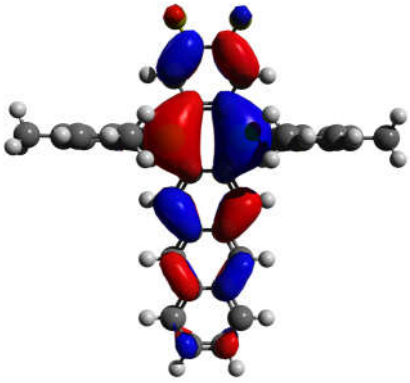
–5.58 eV	–2.42 eV

Scheme S1: Isosurface plots (isovalue: 0.02 $a_0^{-3/2}$) and calculated orbital energy differences for the HOMOs (left) and LUMOs (right).

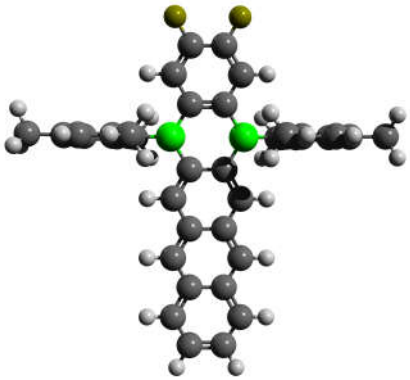

Total energy: -1716.80150518 Hartree
Atom coordinates:

1	6	0	4.746483	0.697592	0.000000
2	6	0	4.746481	-0.697608	0.000001
3	6	0	3.548686	-1.396092	0.000002
4	6	0	2.317713	-0.714316	0.000001
5	6	0	2.317715	0.714309	-0.000001
6	6	0	3.548691	1.396081	-0.000001
7	5	0	0.973861	-1.520542	0.000001
8	6	0	-0.369231	-0.729349	0.000000
9	6	0	-0.369228	0.729351	-0.000001
10	5	0	0.973866	1.520539	-0.000001
11	6	0	-1.576406	-1.398772	0.000001
12	6	0	-2.836050	-0.721439	0.000000
13	6	0	-2.836048	0.721448	-0.000001
14	6	0	-1.576401	1.398777	-0.000001
15	6	0	-4.054757	-1.405101	0.000001
16	6	0	-5.281611	-0.722167	0.000000
17	6	0	-5.281609	0.722185	-0.000001
18	6	0	-4.054752	1.405115	-0.000001
19	6	0	-6.534263	-1.407183	0.000001
20	6	0	-7.716583	-0.712096	0.000000
21	6	0	-7.716581	0.712122	-0.000001
22	6	0	-6.534258	1.407205	-0.000002
23	6	0	0.989856	3.102002	-0.000001
24	6	0	0.989846	-3.102005	0.000001
25	9	0	5.922108	-1.346732	0.000002
26	9	0	5.922113	1.346712	-0.000001
27	6	0	0.997123	3.824758	-1.215184
28	6	0	1.011187	5.223435	-1.197221
29	6	0	1.022138	5.944494	0.000002
30	6	0	1.011185	5.223433	1.197223
31	6	0	0.997120	3.824755	1.215183
32	6	0	0.997109	-3.824758	-1.215183
33	6	0	1.011168	-5.223437	-1.197223
34	6	0	1.022117	-5.944498	-0.000001
35	6	0	1.011167	-5.223439	1.197222
36	6	0	0.997108	-3.824760	1.215183
37	6	0	0.985376	3.094296	2.542684
38	6	0	1.071437	7.454958	0.000003
39	6	0	0.985382	3.094301	-2.542686
40	6	0	0.985367	-3.094304	2.542686
41	6	0	0.985370	-3.094300	-2.542684
42	6	0	1.071410	-7.454961	-0.000003
43	1	0	3.583797	-2.481584	0.000003
44	1	0	3.583805	2.481572	-0.000003
45	1	0	-1.585633	-2.487000	0.000002
46	1	0	-1.585625	2.487005	-0.000001
47	1	0	-4.053335	-2.493211	0.000002
48	1	0	-4.053327	2.493225	-0.000002
49	1	0	-6.531825	-2.494476	0.000001
50	1	0	-8.662911	-1.245885	0.000000
51	1	0	-8.662907	1.245914	-0.000002
52	1	0	-6.531816	2.494498	-0.000002
53	1	0	1.013176	5.763115	-2.143081
54	1	0	1.013172	5.763110	2.143085
55	1	0	1.013154	-5.763115	-2.143084
56	1	0	1.013153	-5.763118	2.143082
57	1	0	0.097641	2.457371	2.645016
58	1	0	0.990912	3.794957	3.383808
59	1	0	1.859866	2.439748	2.650870
60	1	0	0.581433	7.872669	-0.886311
61	1	0	2.107175	7.821082	-0.000020
62	1	0	0.581473	7.872666	0.886340
63	1	0	0.097650	2.457372	-2.645018
64	1	0	1.859875	2.439756	-2.650872
65	1	0	0.990915	3.794962	-3.383809
66	1	0	1.859861	-2.439760	2.650872
67	1	0	0.990901	-3.794966	3.383808
68	1	0	0.097636	-2.457375	2.645019
69	1	0	1.859867	-2.439760	-2.650871
70	1	0	0.097642	-2.457366	-2.645014
71	1	0	0.990898	-3.794960	-3.383808
72	1	0	0.581432	-7.872668	-0.886333
73	1	0	0.581416	-7.872670	0.886318
74	1	0	2.107146	-7.821090	0.000006

9. Device fabrication and measurement of electroluminescence characteristics

All OLEDs were fabricated on glass substrates coated with a patterned transparent ITO (indium tin oxide) conductive layer. The ITO glasses were cleaned by successively sonicating in a detergent solution, distilled water, ethanol, acetone, and isopropanol in an ultrasonic bath. Prior to use, each ITO glass was cleaned by rinsing with acetone and isopropanol. Subsequently, the surface of the ITO substrate was dried for 3 min in an oven at 393 K. After 5 min atmospheric air plasma treatment, using a *Harrick Plasma* PDC-32G-2, 100W Plasma Cleaner, the substrates were loaded into a deposition chamber with a vacuum better than $< 5.0 \times 10^{-4}$ Pa during the evaporation process. All organic materials were thermally evaporated at a deposition rate of 0.2-0.3 Å s^{-1} using a multisource organic molecular vapor deposition system JD400C from *Jiuda Vacuum Technology Co., Ltd*. A LiF layer was deposited at a rate of 0.05 Å s^{-1} and the Al cathode at a rate of 5-8 Å s^{-1}. The thickness of each layer was characterized in advance on a *Bruker* Dektak XT surface profiler. The active area of the diode segments was 2×2 mm^2. The OLED characteristics of all fabricated devices were evaluated at room temperature under nitrogen atmosphere inside a glovebox using a spectrophotometer PR-655, *Photo Research* with a computer controlled programmable direct-current power supply Keithley model 2400 voltage-current source.

After optimizing the OLED device structure, regarding employed materials and thickness of each layer, four devices with different weight percent (%) of the corresponding B-PAH $\mathbf{3^H}$, $\mathbf{3^F}$, and $\mathbf{3^{Cl}}$ in the emissive layer were fabricated (2%, 5%, 10%, and 15%). The structure of these devices are following: indium tin oxide (ITO, 135 nm)/dipyrazino[2,3-*f*:2',3'-*h*]quinoxaline-2,3,6,7,10,11-hexacarbonitrile (HATCN, 3.5 nm)/*N*,*N*'-di(1-naphthyl)-*N*,*N*'-diphenyl-(1,1'-biphenyl)-4,4'-diamine (NPB, 30.8 nm)/9,10-di-(2-naphthyl)anthracene (ADN, 7.5 nm) doped with different wt% of the corresponding B-PAH $\mathbf{3^{H/F/Cl}}$/1,3,5-tris(1-phenyl-1*H*-benzo[*d*]imidazol-2-yl)benzene (TPBi, 18 nm)/LiF (1 nm)/Al (120 nm).

9.1 Electroluminescence characteristics of neat ADN in the emissive layer

Table S3. Electroluminescent characteristics of neat ADN in the emissive layer.

EL λ_{max}[a] (nm)	V_{on}[b] (V)	L_{max}[c] (cd m^{-2})	η_{ext}[d] (%)				max. η_c[e] (cd A^{-1})	max. η_p[f] (lm W^{-1})	CIE[a,g] (x, y)
			max.	10 cd m^{-2}	100 cd m^{-2}	1000 cd m^{-2}			
432	4.2	5083 @ 8V	2.0	0.4	1.8	1.9	2.5	1.3	(0.16, 0.10)

[a] Value taken at 9 V. [b] V_{on}: voltage required to turn-on a luminance of 1 cd m^{-2}. [c] L_{max}: maximum luminance. [d] η_{ext}: external quantum efficiency. [e] η_c: current efficiency. [f] η_p: power efficiency. [g] CIE coordinates 1931.

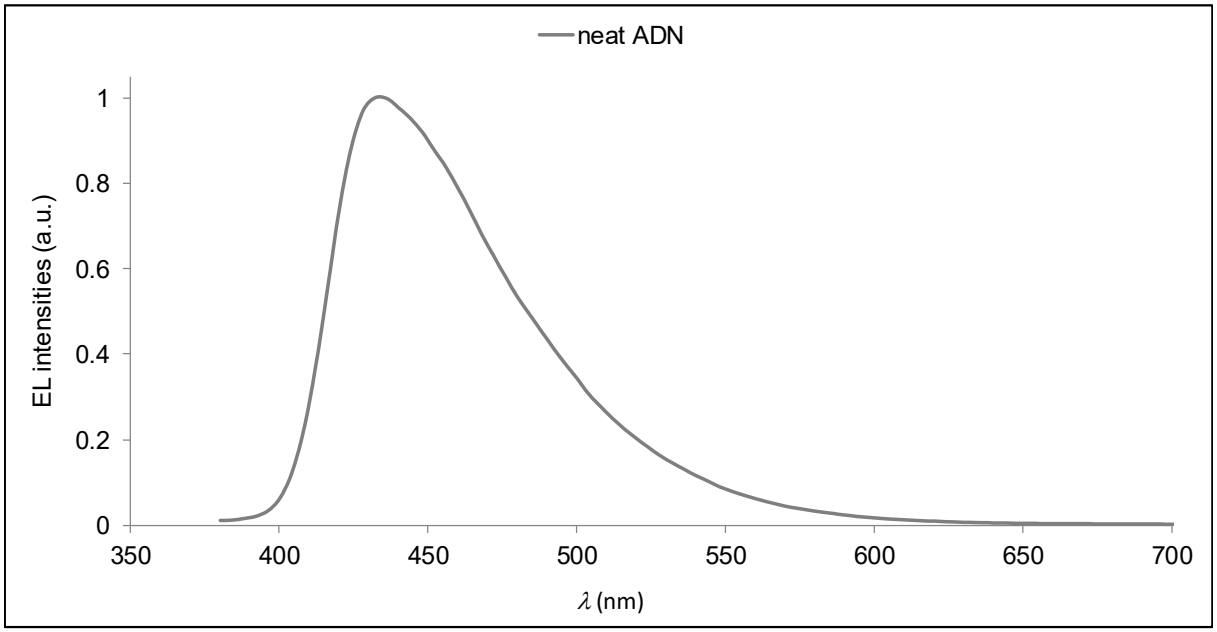

Figure S15: Normalized electroluminescent spectra of neat ADN in the EML. *Note:* An electroluminescent spectrum with a luminance around 5000 cd m^{-2} was chosen.

9.2 Electroluminescence characteristics of 3^{H}

Table S4. Electroluminescence characteristics of devices with different thicknesses of the EML (ADN doped with 5% **3^{H}**; entries 1-4) and the charge-transport layers (HIL/HTL/ETL ; entries 5-6).

#	different thickness of:	anode	HIL (nm)	HTL (nm)	EML (nm)	ETL (nm)	cathode	V_{on}[a] (V)	L_{max}[b] (cd m^{-2})	max. η_{ext}[c] (%)
1	EML	ITO	HATCN (3.5)	NPB (30.8)	5% **3^{H}** in ADN (22.5)	TPBi (18)	LiF/Al	5.8	39300 @ 13.5V	3.3
2		ITO	HATCN (3.5)	NPB (30.8)	5% **3^{H}** in ADN (11.3)	TPBi (18)	LiF/Al	4.5	29500 @ 11V	3
3		ITO	HATCN (3.5)	NPB (30.8)	5% **3^{H}** in ADN (7.5)	TPBi (18)	LiF/Al	3.6	26080 @ 9V	2.9
4		ITO	HATCN (3.5)	NPB (30.8)	5% **3^{H}** in ADN (3.8)	TPBi (18)	LiF/Al	3.9	18060 @ 9V	2.3
5	HIL/HTL/ ETL	ITO	-	NPB (30.8)	5% **3^{H}** in ADN (7.5)	TPBi (18)	LiF/Al	5.4	20420 @ 8.5V	2.8
6		ITO	HATCN (3.5)	NPB (46.2)	5% **3^{H}** in ADN (7.5)	TPBi (24)	LiF/Al	5.2	33070 @ 12V	3.2

[a] V_{on}: voltage required to turn-on a luminance of 1 cd m^{-2}. [b] L_{max}: maximum luminance and required driving voltage. [c] η_{ext}: external quantum efficiency. Abbreviations: HIL: hole-injection layer; HTL: hole-transport layer; EML: emissive layer (incorporates a host material in which an emitter is introduced as a dopant); ETL: electron-transport layer.

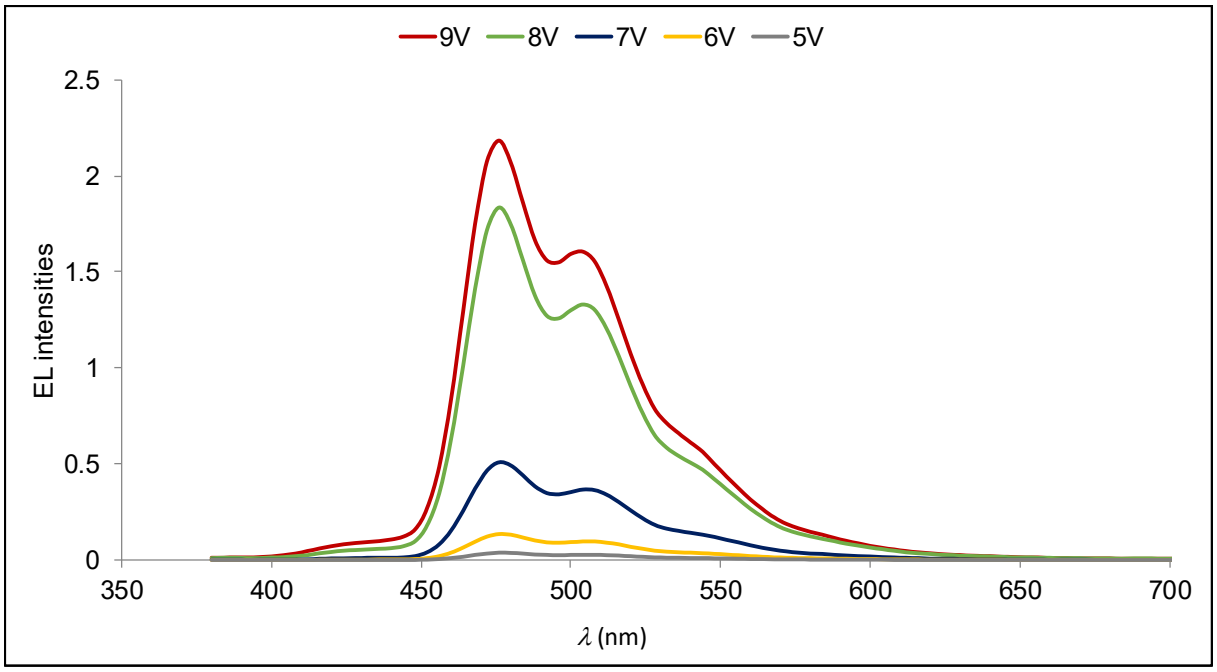

Figure S16: Electroluminescent spectra of the device **A** (2% **3^{H}**) at various driving voltages.

9.3 Electroluminescence characteristics of 3^{F}

Table S5. Electroluminescent characteristics of the B-PAH **3^{F}**.

Device	EL[a] λ_{max} (nm)	V_{on}[b] (V)	L_{max}[c] (cd m^{-2})	η_{ext}[d] (%)				max. η_c[e] (cd A^{-1})	max. η_p[f] (lm W^{-1})	CIE[a] (x, y)
				max.	10 cd m^{-2}	100 cd m^{-2}	1000 cd m^{-2}			
E: 2% 3^{F}	484	3.8	23000 @ 8.6V	2.5	1.9	2.1	2.4	6.4	3.8	(0.18, 0.45)
F: 5% 3^{F}	488	4.3	23210 @ 9.5V	2.0	1.7	1.8	2.0	5.6	3.4	(0.19, 0.49)
G: 10% 3^{F}	492	4.3	14510 @ 10V	1.4	1.2	1.4	1.3	4.1	2.3	(0.21, 0.52)
H: 15% 3^{F}	492	4.4	10880 @ 8.5V	1.1	1.0	1.1	1.1	3.3	1.9	(0.22, 0.52)

[a] value taken at 9 V. [b] V_{on}: voltage required to turn-on a luminance of 1 cd m^{-2}. [c] L_{max}: maximum luminance. [d] η_{ext}: external quantum efficiency. [e] η_c: current efficiency. [f] η_p: power efficiency.

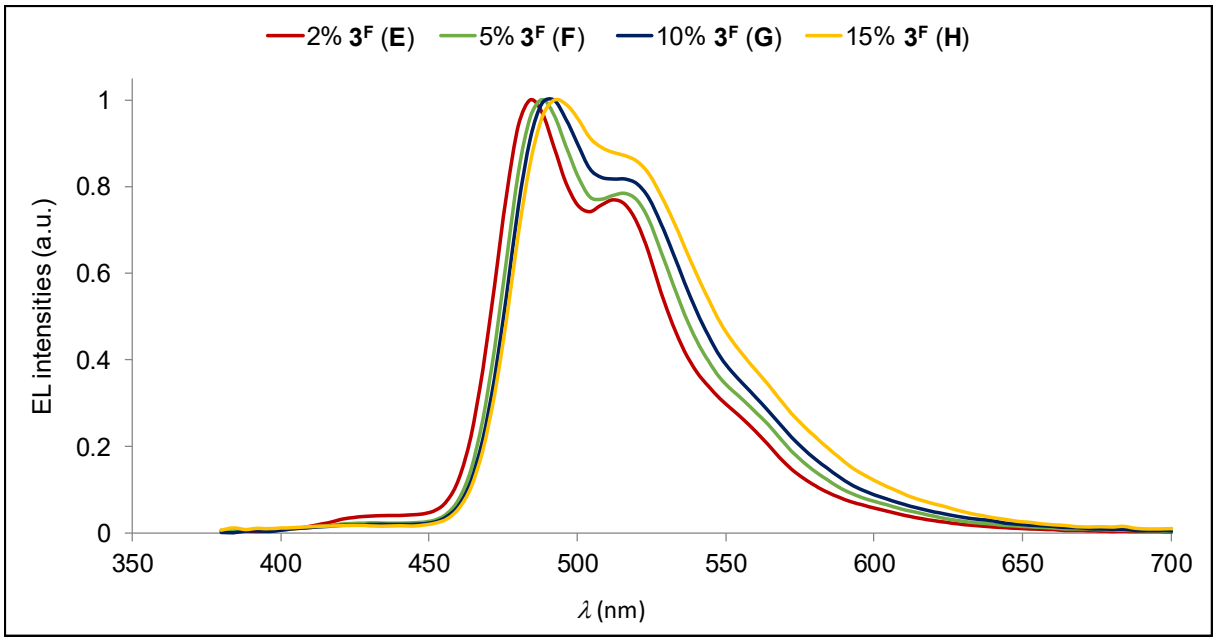

Figure S17: Normalized electroluminescent spectra with different % of the dopant **3F** in the EML. *Note:* For each % of **3F** an electroluminescent spectrum with a luminance around 10000 cd m^{-2} was chosen.

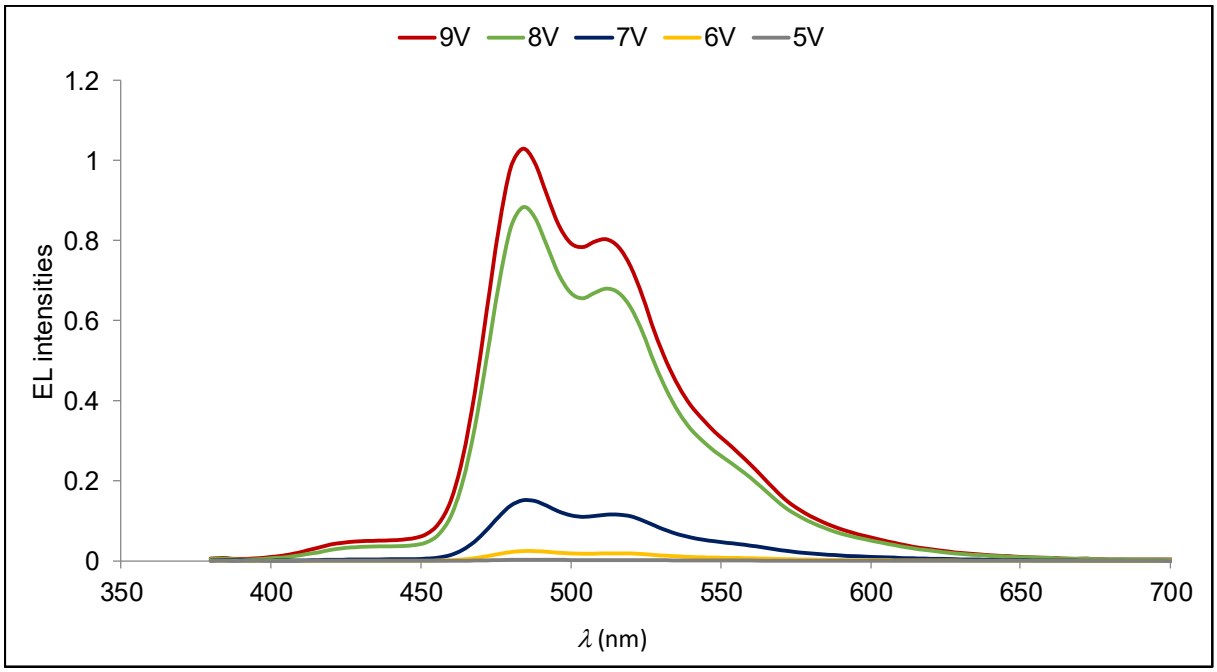

Figure S18: Electroluminescent spectra of the device **E** (2% **3F**) at various driving voltages.

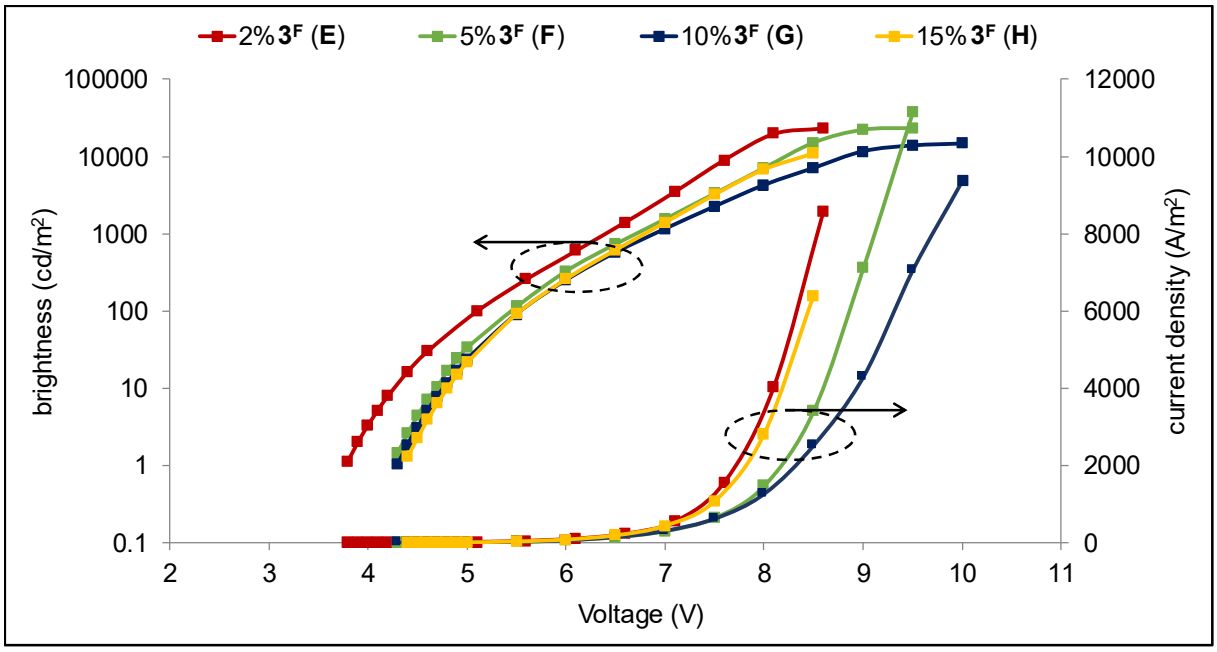

Figure S19: *L-J-V* characteristics of the devices **E** (2% **3F**), **F** (5% **3F**), **G** (10% **3F**), and **H** (15% **3F**).

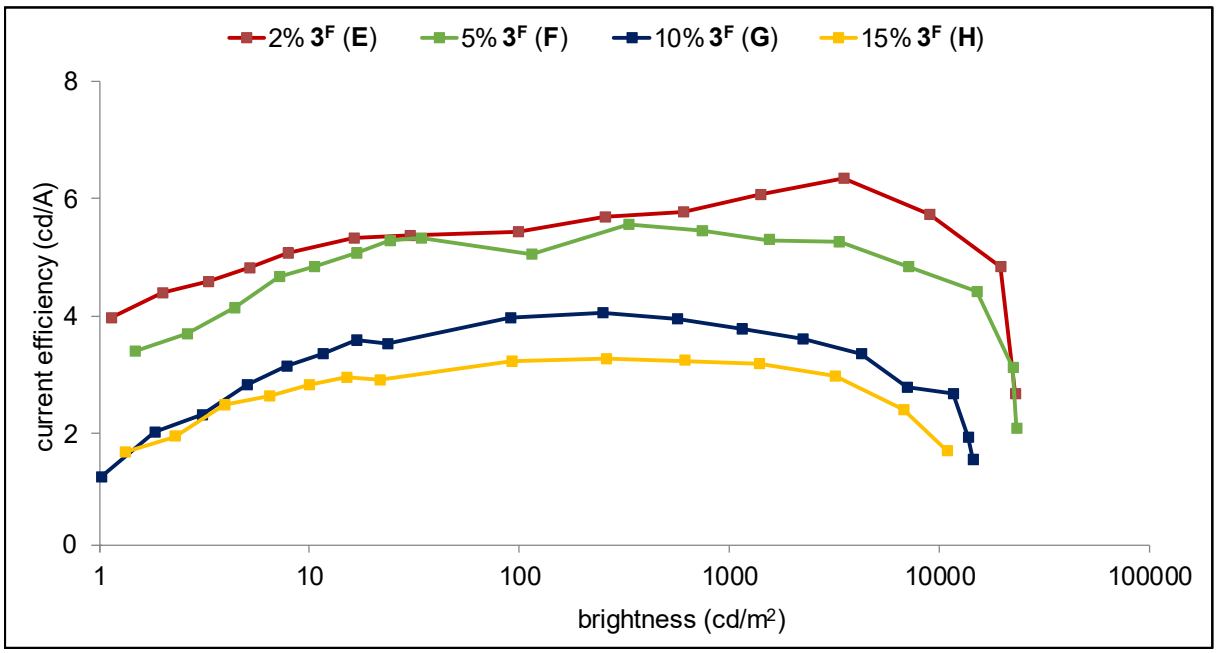

Figure S20: Current efficiency-*L* characteristics of the devices **E** (2% **3F**), **F** (5% **3F**), **G** (10% **3F**), and **H** (15% **3F**).

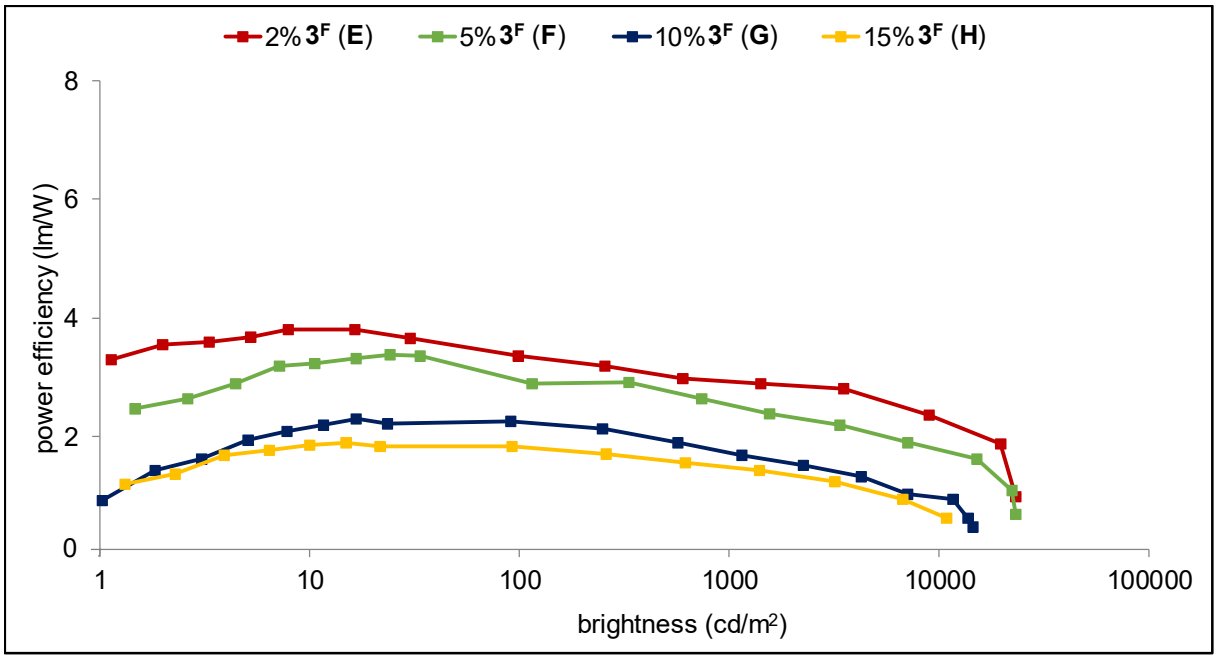

Figure S21: Power efficiency-*L* characteristics of the devices **E** (2% **3**^{F}), **F** (5% **3**^{F}), **G** (10% **3**^{F}), and **H** (15% **3**^{F}).

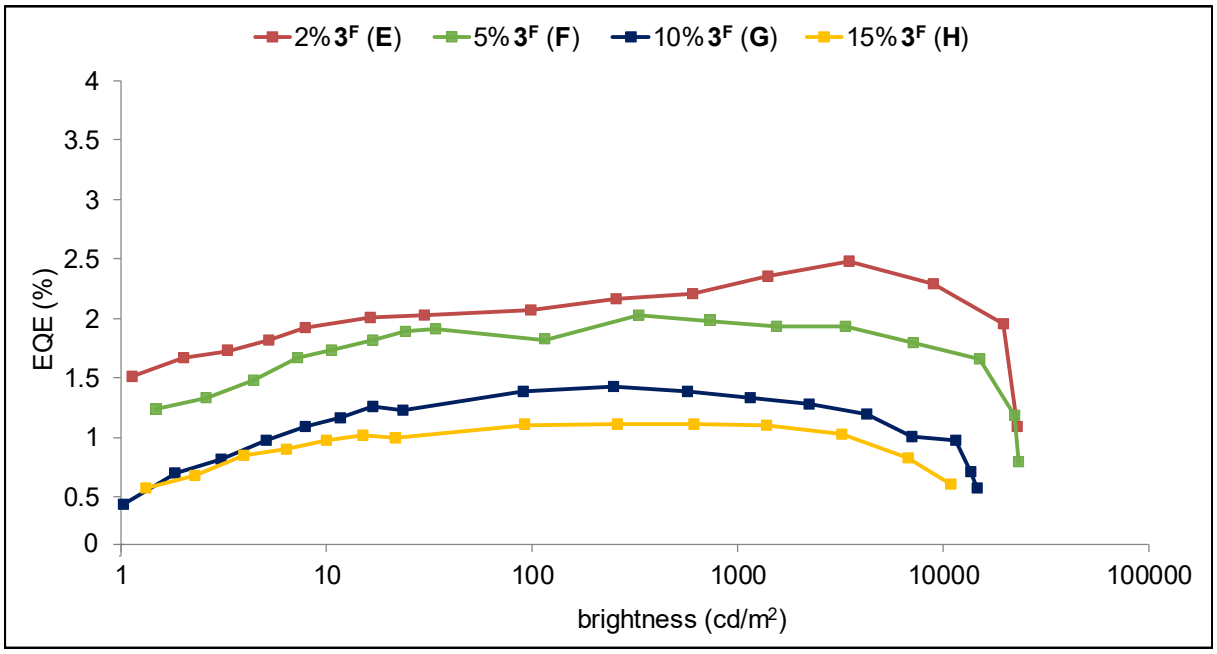

Figure S22: External quantum efficiency (EQE)-*L* characteristics of the devices **E** (2% **3**^{F}), **F** (5% **3**^{F}), **G** (10% **3**^{F}), and **H** (15% **3**^{F}).

9.4 Electroluminescence characteristics of 3^{Cl}

Table S6. Electroluminescent characteristics of the B-PAH $\mathbf{3^{Cl}}$.

Device	EL[a] λ_{max} (nm)	V_{on}[b] (V)	L_{max}[c] (cd m^{-2})	η_{ext}[d] (%)				max. η_c[e] (cd A^{-1})	max. η_p[f] (lm W^{-1})	CIE[a] (x, y)
				max.	10 cd m^{-2}	100 cd m^{-2}	1000 cd m^{-2}			
I: 2% 3^{Cl}	492	3.3	26620 @ 8.5V	2.8	2.5	2.5	2.6	7.9	5.8	(0.20, 0.51)
J: 5% 3^{Cl}	500	4.1	22090 @ 10.5V	2.3	1.7	2.2	2.1	7.1	4.3	(0.24, 0.58)
K: 10% 3^{Cl}	500	4.2	15300 @ 9.5V	1.6	1.2	1.5	1.6	5.0	2.8	(0.25, 0.59)
L: 15% 3^{Cl}	504	4.2	14320 @ 9V	1.3	0.9	1.3	1.3	4.1	2.4	(0.26, 0.58)

[a] value taken at 9 V. [b] V_{on}: voltage required to turn-on a luminance of 1 cd m^{-2}. [c] L_{max}: maximum luminance. [d] η_{ext}: external quantum efficiency. [e] η_c: current efficiency. [f] η_p: power efficiency.

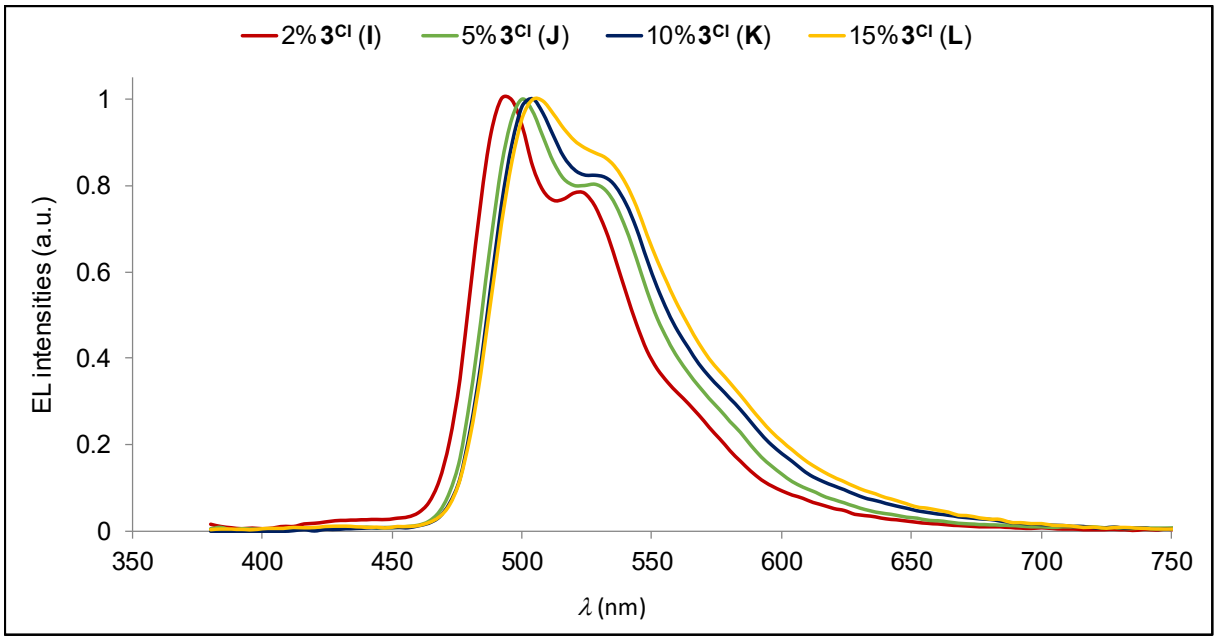

Figure S23: Normalized electroluminescent spectra with different % of the dopant $\mathbf{3^{Cl}}$ in the EML. *Note:* For each % of $\mathbf{3^{Cl}}$ an electroluminescent spectrum with a luminance around 1000 cd m^{-2} was chosen.

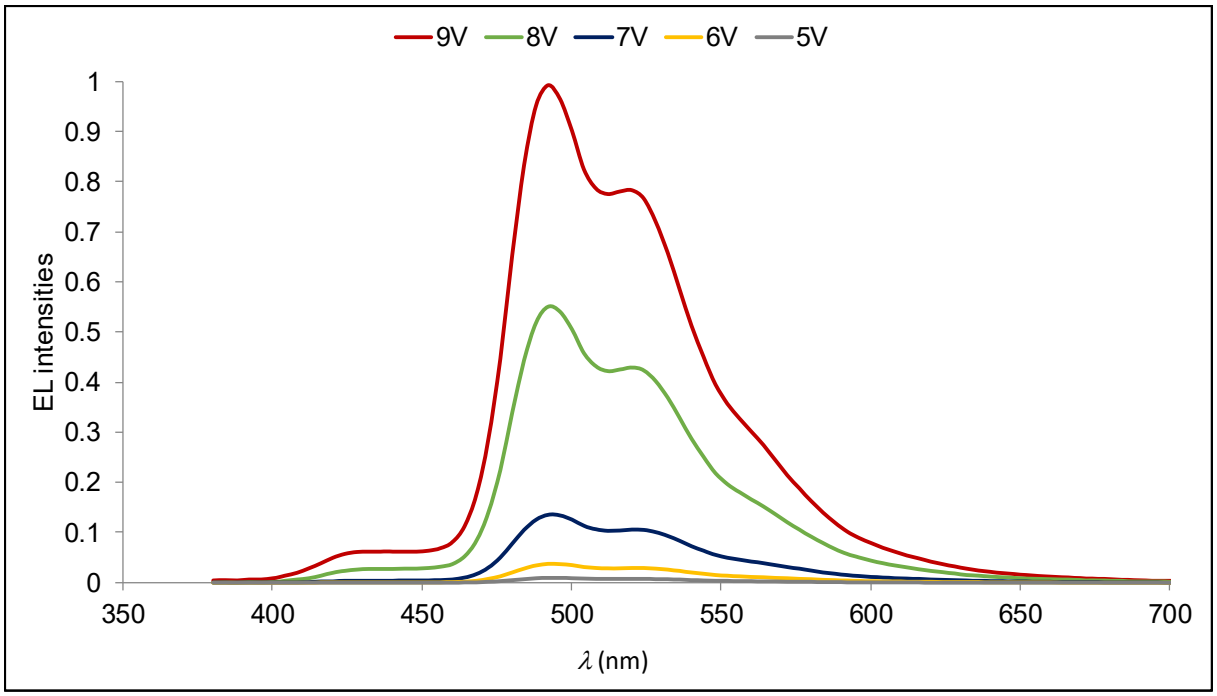

Figure S24: Electroluminescent spectra of the device **I** (2% **3**^{Cl}) at various driving voltages.

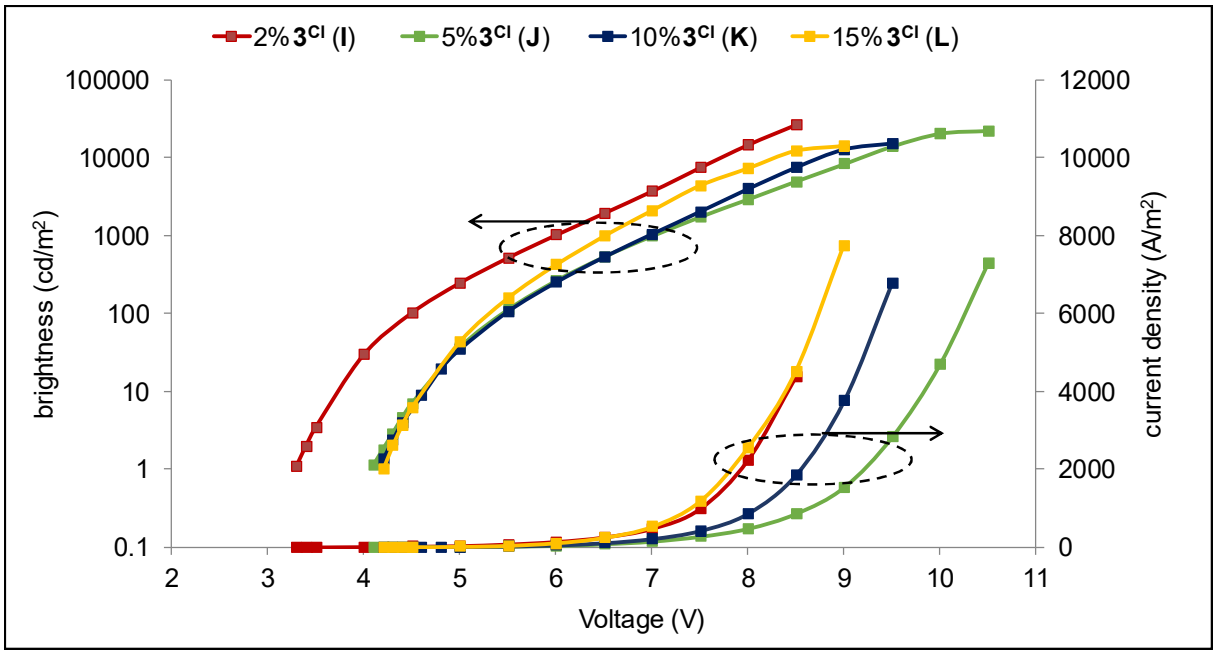

Figure S25: *L-J-V* characteristics of the devices **I** (2% **3**^{Cl}), **J** (5% **3**^{Cl}), **K** (10% **3**^{Cl}), and **L** (15% **3**^{Cl}).

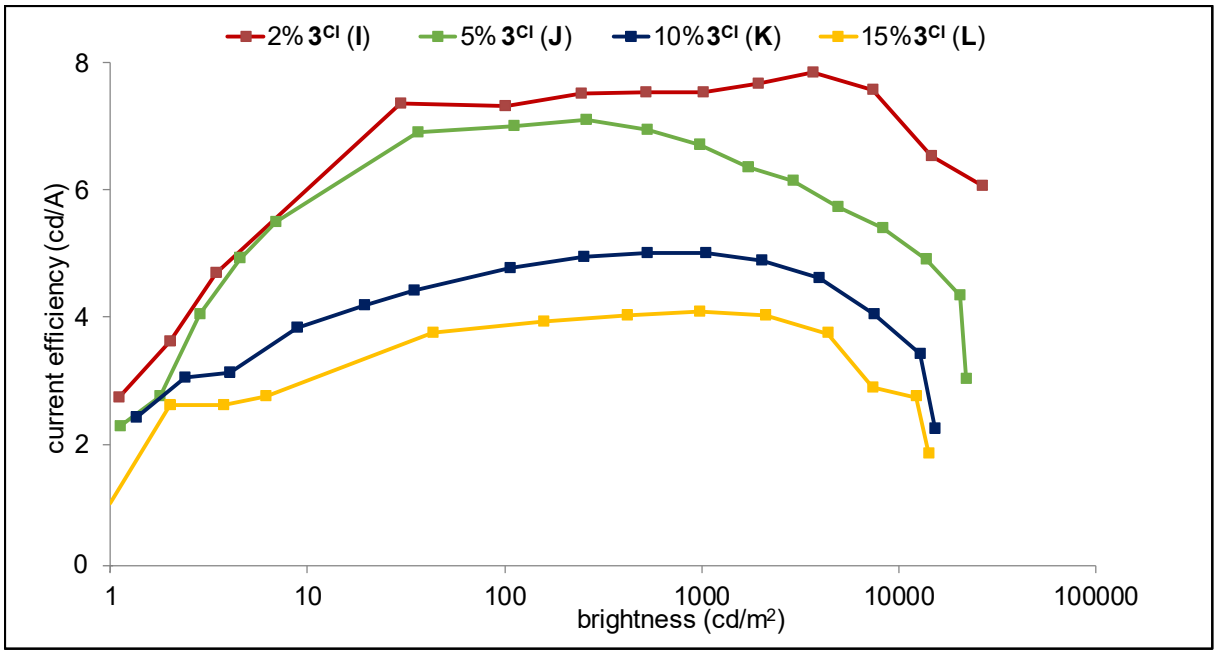

Figure S26: Current efficiency-*L* characteristics of the devices **I** (2% **3**^{Cl}), **J** (5% **3**^{Cl}), **K** (10% **3**^{Cl}), and **L** (15% **3**^{Cl}).

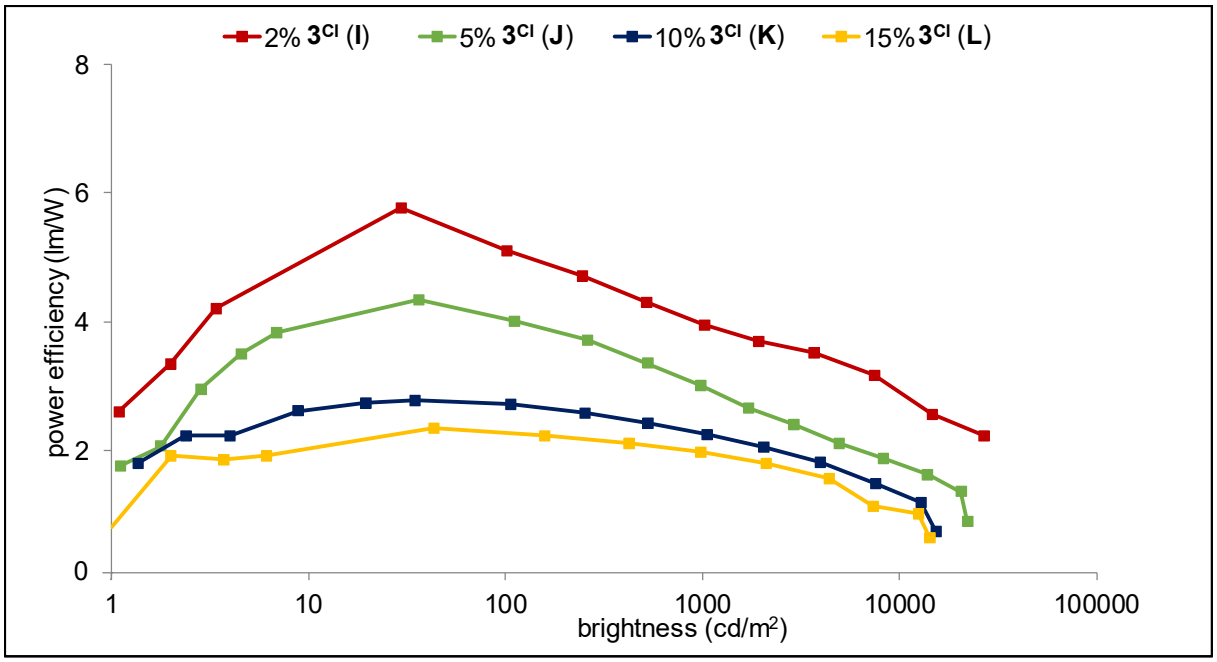

Figure S27: Power efficiency-*L* characteristics of the devices **I** (2% **3**^{Cl}), **J** (5% **3**^{Cl}), **K** (10% **3**^{Cl}), and **L** (15% **3**^{Cl}).

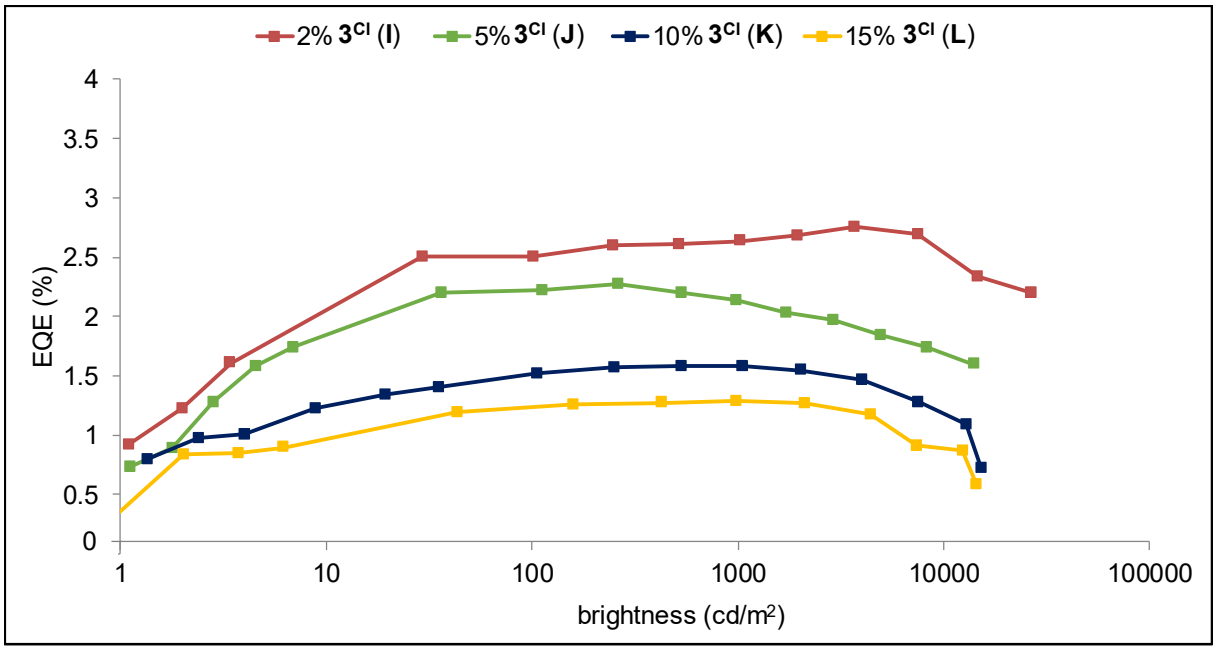

Figure S28: External quantum efficiency (EQE)-*L* characteristics of the devices **I** (2% **3**^{Cl}), **J** (5% **3**^{Cl}), **K** (10% **3**^{Cl}), and **L** (15% **3**^{Cl}).

10. Thermogravimetric analysis (TGA)

The thermogravimetric analysis was performed on a *Shimadzu DTG-60AH* DTA-TG apparatus with a heating rate of 10 °C min^{-1} under an atmosphere of nitrogen.

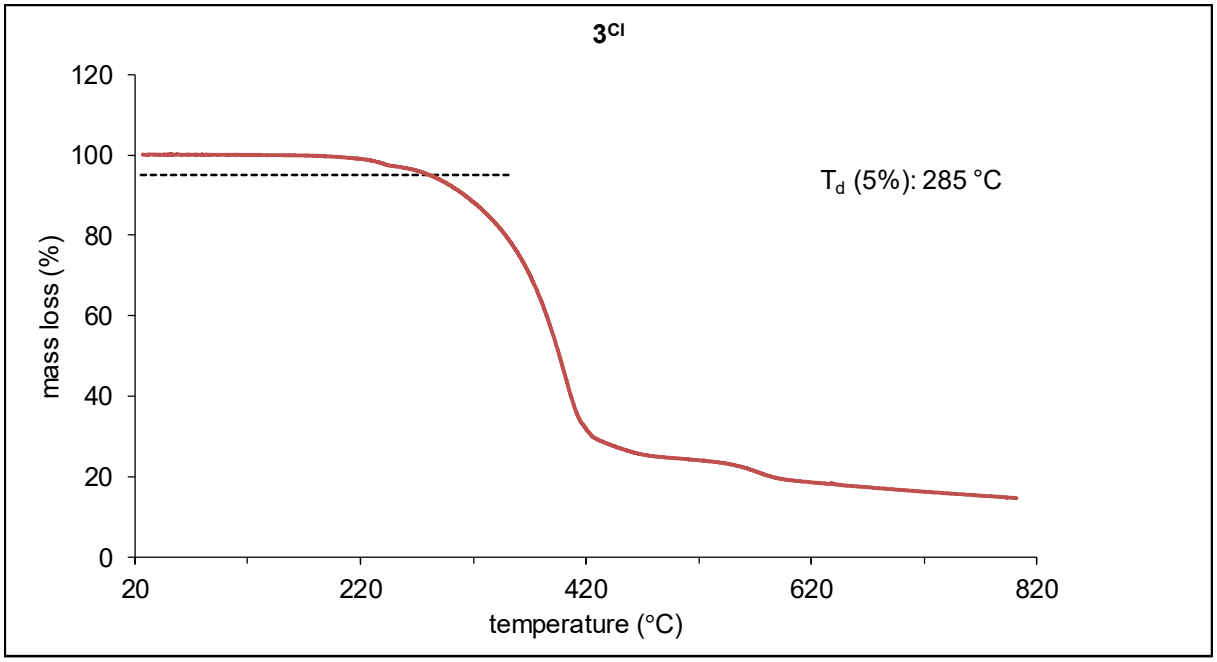

Figure S29: TGA curve of **3Cl**. T_d (5%) refers to the temperature at which a 5% mass loss had occurred.

11. References

[S1] T. Kitamura, R. Yamada, K. Gondo, N. Eguchi, J. Oyamada, *Synthesis*, 2017, **49**, 2495-2500. Note: We prepared the compound analogous to 4-fluoro-1,2-bis(trimethylsilyl)benzenes as described in: A. Lorbach, C. Reus, M. Bolte, H.-W. Lerner, M. Wagner, *Adv. Synth. Catal.*, 2010, **352**, 3443-3449.

[S2] A. John, M. Bolte, H.-W. Lerner, M. Wagner, *Angew. Chem. Int. Ed.*, 2017, **56**, 5588-5592.

[S3] K. Suzuki, A. Kobayashi, S. Kaneko, K. Takehira, T. Yoshihara, H. Ishida, Y. Shiina, S. Oishic, S. Tobita, *Phys. Chem. Chem. Phys.*, 2009, **11**, 9850-9860.

[S4] A. M. Brouwer, *Pure Appl. Chem.*, 2011, **83**, 2213-2228.

[S5] T.-S. Ahn, R.O. Al-Kaysi, A. M. Müller, K. M. Wentz, C. Bardeen, *J. Rev. Sci. Instrum.*, 2007, **78**, 086105.

[S6] H. Nöth, B. Wrackmeyer, *Nuclear Magnetic Resonance Spectroscopy of Boron Compounds*. In *NMR Basic Principles and Progress*, Springer, Berlin, 1978.

[S7] Stoe & Cie, *X-AREA. Diffractometer control program system.* Stoe & Cie, Darmstadt, Germany, 2002.

[S8] G. M. Sheldrick, *Acta Crystallogr. Sect. A*, 2008, **64**, 112-122.

[S9] Gaussian 09, Revision D.01, M. J. Frisch, G. W. Trucks, H. B. Schlegel, G. E. Scuseria, M. A. Robb, J. R. Cheeseman, G. Scalmani, V. Barone, B. Mennucci, G. A. Petersson, H. Nakatsuji, M. Caricato, X. Li, H. P. Hratchian, A. F. Izmaylov, J. Bloino, G. Zheng, J. L. Sonnenberg, M. Hada, M. Ehara, K. Toyota, R. Fukuda, J. Hasegawa, M. Ishida, T. Nakajima, Y. Honda, O. Kitao, H. Nakai, T. Vreven, J. A. Montgomery, Jr., J. E. Peralta, F. Ogliaro, M. Bearpark, J. J. Heyd, E. Brothers, K. N. Kudin, V. N. Staroverov, T. Keith, R. Kobayashi, J. Normand, K. Raghavachari, A. Rendell, J. C. Burant, S. S. Iyengar, J. Tomasi, M. Cossi, N. Rega, J. M. Millam, M. Klene, J. E. Knox, J. B. Cross, V. Bakken, C. Adamo, J. Jaramillo, R. Gomperts, R. E. Stratmann, O. Yazyev, A. J. Austin, R. Cammi, C. Pomelli, J. W. Ochterski, R. L. Martin, K. Morokuma, V. G. Zakrzewski, G. A. Voth, P. Salvador, J. J. Dannenberg, S. Dapprich, A. D. Daniels, O. Farkas, J. B. Foresman, J. V. Ortiz, J. Cioslowski, and D. J. Fox, Gaussian, Inc., Wallingford, CT, USA, 2013.